17

The Effect of Moisture on the Adhesion and Fracture of Interfaces in Microelectronic Packaging

Timothy P. Ferguson[a] and Jianmin Qu[b]

[a]*Southern Research Institute, 757 Tom Martin Drive, Birmingham, AL 35211, USA*

[b]*G.W. Woodruff School of Mechanical Engineering, Georgia Institute of Technology, Atlanta, GA 30332-0405, USA*

Abstract

A significant problem in the microelectronic packaging industry is the presence of moisture-induced failure mechanisms. Moisture is a multi-dimensional concern in packaging, having an adverse effect on package reliability by introducing corrosion, development of hygro-stresses, and degradation of polymers present in the package. Moisture can also accelerate delamination by deteriorating the polymer interfaces within the package. As the interfacial adhesion between the chip, underfill, and substrate decreases, the likelihood of delamination at each encapsulant interface increases. Once the package delaminates, the solder joints in the delaminated area are exposed to high stress concentrations, resulting in a reduction of overall package life.

Moisture can affect interfacial adhesion through two primary mechanisms. The first mechanism is the direct presence of moisture at the interface altering the interfacial integrity of the adhesive joint. The second mechanism is the absorbed moisture in either the adhesive and/or substrate altering the mechanical properties of those materials, which changes the response of the adhesive structure in the presence of an externally applied load. Inevitably, the effect of moisture on the adhesion and fracture of interfaces entails a multi-disciplinary study, and several aspects should be considered. From a global perspective, the primary aspects include moisture transport behavior, changes in bulk material properties from moisture absorption, effect of moisture on interfacial adhesion, and recovery from moisture upon fully drying, although several subsections within each major group occur due to the complexity of the problem.

In this chapter, a systematic and multi-disciplinary study is presented to address the fundamental science of moisture-induced degradation of interfacial adhesion. First, the

moisture transport behavior within underfill adhesives is experimentally characterized. The results are incorporated into a finite element model to depict the moisture ingress and interfacial moisture concentration after moisture preconditioning. Second, the effect of moisture on the variation of the adhesive elastic modulus is demonstrated and the physical mechanisms for the change identified. Third, the aggregate effect of moisture on the interfacial fracture toughness is determined. This includes the primary effect of moisture being physically present at the interface and the secondary effect of moisture changing the elastic modulus of the adhesive when absorbed. Both reversible and irreversible components of the interfacial moisture degradation are evaluated. Using adsorption theory in conjunction with fracture mechanics, an analytical model is developed that predicts the loss in interfacial fracture toughness as a function of moisture content. The model incorporates key parameters relevant to the problem of moisture in epoxy joints identified from the experimental portion of this research, including the interfacial hydrophobicity, active nanopore density, saturation concentration, and density of water.

17.1. INTRODUCTION

It is inevitable that an electronic device will be exposed to varying degrees of moisture. Since many microelectronic packages utilize epoxy based materials such as underfill and molding compounds, they are highly susceptible to moisture absorption. The moisture uptake can lead to undesirable changes in mechanical performance, interfacial adhesion, and reliability [46,50].

Long term reliability and life prediction of microelectronic assemblies requires a rooted understanding in the interfacial failure mechanisms and associated debonding behavior of adhesive joints within these assemblies. With the advent of flip-chip technology, the need for improved understanding of delamination in these assemblies has taken on added importance. One of the keys to the success of flip-chip technology lies in development of underfill, which is an epoxy-based encapsulant that mechanically couples the chip to the board. Underfill drastically enhances the reliability of microelectronic assembles when compared to unencapsulated devices [51], provided the structural integrity of the adhesive bond is maintained. Although delamination of the underfill in the microelectronic assembly tends to cause near immediate failure as soon as it reaches a solder joint, until recently the factors that affect the strength and durability of these interfaces have not been investigated and are the focal points of current studies in reliability research in microelectronic packaging. One of the most detrimental of these factors is moisture, which can significantly compromise the interfacial adhesion and accelerate the onset of delamination.

Another major area of concern in microelectronic packaging occurs at the interface between the copper alloy lead frame and the epoxy mold compound. Due to its relatively low cost in conjunction with its high electrical and thermal conductivity, copper alloys are widely used as a lead frame material. However, the epoxy/copper interface has poor interfacial adhesion strength and relatively high residual stress, which predisposes it to delamination. The copper surface is also highly susceptible to oxidation, which is an additional consideration when evaluating the interfacial adhesion of interfaces involving copper [9,28]. The delamination between the copper lead frame and the mold compound adversely affects the durability of these packages and is a common failure mode during the qualification process. In addition to further compromising the interfacial integrity of the interface, the delamination can also affect long term package reliability by yielding enhanced transport

of moisture along the interface resulting in corrosion. The corrosion process will be accelerated if the absorbed moisture is a carrier of ionic impurities from the surrounding external environment [62]. Consequently, the epoxy/copper interface is another significant area of concern in microelectronic packaging reliability. Several studies continue to investigate this topic to better understand the durability and failure mechanisms, including the loss of adhesion in the presence of moisture.

17.2. MOISTURE TRANSPORT BEHAVIOR

17.2.1. Background

Central to understanding the effect of moisture on interfacial adhesion is to first identify the rate at which moisture is delivered to the interface. The three primary parameters that have the greatest effect on diffusion rates are the size of the diffusing particles, temperature, and viscosity of the environment. Lighter particles have a higher velocity for the same kinetic energy as heavier particles, thus lighter particles diffuse faster than heavier particles. Similarly, an increase in temperature will produce a higher kinetic energy yielding an increase in velocity, thus particles will diffuse more rapidly at elevated temperatures. Last, diffusion is more rapid in a gas than in a solid as a result of less atomic interactions, which retard the diffusion process.

Since the vast majority of underfills are epoxy based, they are highly susceptible to moisture absorption. A standard epoxy formulation can absorb between 1 and 7 wt% moisture [48]. Additional considerations that apply specifically to moisture absorption in epoxies include the epoxy surface topology and resin polarity. Soles et al. [47] have found that water initially enters the epoxy network through the nanopores that are inherent in the epoxy surface topology. They have determined the average size of a nanopore diameter to vary from 5.0 to 6.1 Å and account for 3–7% of the total volume of the epoxy material. Since the approximate diameter of a kinetic water molecule is just 3.0 Å, moisture can easily traverse into the epoxy via the nanopores.

Although surface topology can influence moisture penetration into an epoxy, of primary importance is the resin polarity, with the high polarity of the water molecule being susceptible to specific epoxy–water interactions. Less polar resins such as non-amine resins have more enhanced moisture diffusion coefficients than amine-containing resins. Soles and Yee [48] have shown that polar sites, such as amine functional groups, provide low energy wells for the water molecules to attach. Consequently, polar hydroxyls and amines can regulate transport through the nanopores by either blocking or allowing moisture to traverse the epoxy resin depending on the orientation of the resin with respect to nanopore position. Conversely, the absence of hydroxyls and amines in a non-amine resin leads to an enhanced moisture diffusion coefficient. In addition, non-amine resins absorb very little water relative to more polar resins, such as amine resins. Soles and Yee [48] have shown that by increasing the cross-link density, the intrinsic hole volume fraction is increased, which yields an increase in the equilibrium moisture content. Steric hindrances located at cross-link junctions open the epoxy matrix to facilitate interactions of water with polar groups, thus increasing the moisture uptake. Depending on the various chemical conformations of the epoxy resin in association with the inherent nanopores present in the epoxy structure, water molecules will behave differently in various epoxy resins.

17.2.2. Diffusion Theory

Since the transfer of heat by conduction is also attributed to random molecular motions, it is clear that diffusion is analogous to heat conduction. Fick adopted Fourier's mathematical expression for heat conduction to quantify diffusion. Fick's first law states that the rate of transfer of diffusing particles per plane of unit area is proportional to the concentration gradient measured normal to the plane:

$$F_x = -D\frac{\partial C}{\partial x}, \tag{17.1}$$

where F_x is the diffusion flux in the x direction, D is the diffusion coefficient, and $\partial C/\partial x$ is the concentration gradient. The negative sign in the above expression accounts for the fact that diffusion occurs in the opposite direction of increasing concentration. In addition, the expression is only valid for an isotropic medium.

Fick's second law of diffusion describes the nonsteady state diffusion of a substance and can be derived using Equation (17.1). Utilizing Equation (17.1) and a differential volume element in Cartesian coordinates, Crank [11] has shown that the following expression can be obtained assuming a constant diffusion coefficient:

$$\frac{\partial C}{\partial t} = D\left(\frac{\partial^2 C}{\partial x^2} + \frac{\partial^2 C}{\partial y^2} + \frac{\partial^2 C}{\partial z^2}\right), \tag{17.2}$$

where C is the concentration of the diffusing substance and D is the diffusion coefficient. For one-dimensional diffusion along the x-axis, the previous relation reduces to the following form:

$$\frac{\partial C}{\partial t} = D\left(\frac{\partial^2 C}{\partial x^2}\right). \tag{17.3}$$

The solution of Equation (17.3) for the concentration of a diffusing substance in an isotropic plane sheet of finite thickness as a function of time and space is given by [11]:

$$\frac{C(x,t)}{C_1} = 1 - \frac{4}{\pi}\sum_{n=0}^{\infty}\frac{(-1)^n}{2n+1}\exp\left[\frac{-D(2n+1)^2\pi^2 t}{4\ell^2}\right]\cos\frac{(2n+1)\pi x}{2\ell}, \tag{17.4}$$

where D is the diffusion coefficient, ℓ is the half-thickness of the sheet ($-\ell < x < \ell$), C is concentration of the diffusing substance absorbed by the sample at position x and time t, and C_1 is the saturation concentration of the absorbed substance. The application of Equation (17.4) assumes that immediately after the sheet is placed in the vapor both surfaces obtain a concentration that is equivalent to the equilibrium uptake, remaining constant. In addition the equation assumes that the diffusion coefficient remains constant throughout the diffusion process and that the initial concentration of the diffusing substance in the specimen is zero. An analogous expression given on a mass basis has been shown by Crank [11] to be the following:

$$\frac{M_t}{M_\infty} = 1 - \frac{8}{\pi^2}\sum_{m=0}^{\infty}\frac{1}{(2m+1)^2}\exp\left[\frac{-D(2m+1)^2\pi^2 t}{h^2}\right], \tag{17.5}$$

where D is the diffusion coefficient, h is the total sheet thickness, M_t is total mass of the diffusing substance absorbed by the sample at time t, and M_∞ is the equilibrium mass of the absorbed substance. In the initial stages of absorption where $M_t/M_\infty < 1/2$ and assuming a constant diffusion coefficient, D, Equation (17.5) can be shown to be approximated by the following:

$$\frac{M_t}{M_\infty} = \frac{4}{h}\sqrt{\frac{Dt}{\pi}}. \tag{17.6}$$

If absorption data is plotted with M_t/M_∞ as a function of $(t/h^2)^{1/2}$ and exhibits linear behavior for $M_t/M_\infty < 1/2$, the diffusion coefficient can be determined by rearranging Equation (17.6) to the following form:

$$D = \frac{\pi}{16}\left(\frac{M_t/M_\infty}{\sqrt{t}/h}\right)^2. \tag{17.7}$$

The diffusivity, D, can now be experimentally determined using absorption data with Equation (17.7). Again, Equations (17.4), (17.5), (17.6), and (17.7) all assume that the one-dimensional absorption occurs on both sides of the plane sheet with a concentration-independent, constant diffusivity. If absorption results in a diffusion coefficient that is variable rather than constant, explicit analytical solutions are no longer available.

17.2.3. Underfill Moisture Absorption Characteristics

Being epoxy-based, underfill resins are highly susceptible to moisture ingress. It is important to ascertain the fundamental moisture absorption behavior of each underfill when evaluating reliability performance in moist environments. In the case of adhesion testing, it is essential to accurately quantify the change in adhesion for a particular interfacial moisture concentration. This provides insight into the constitutive behavior of adhesion in the presence of moisture.

Two no-flow underfills were evaluated to determine their absorption behavior to select an ideal candidate for a fundamental study in the effect of moisture on interfacial adhesion. Underfill resin A (UR-A) was developed at the Georgia Institute of Technology. Underfill resin B (UR-B) was supplied by a commercial manufacturer. It should be noted that since both underfills were formulated for no-flow assembly, neither contained any filler content. Test samples were made approximately 60 mm in diameter and 2 mm thick, hence promoting predominately one-dimensional diffusion through the thickness of the sample. The samples were baked at 115°C for at least 12 hours to remove moisture prior to being placed into a humidity chamber for moisture preconditioning. The atmosphere within the humidity chamber was maintained at a constant temperature (85 ± 1°C), humidity (85 ± 1%RH), and pressure (P_{atm}). Moisture uptake profiles for each underfill are shown in Figures 17.1 and 17.2.

It is evident from Figures 17.1 and 17.2 that UR-A had not reached saturation after 168 hours of exposure, whereas UR-B had approached a saturated state within the same timeframe. In fact, samples constructed from UR-A did not reach saturation even after 725 hours of exposure. This absorption behavior is not uncommon, with Vanlandingham et al. [54] noting that some of the epoxies evaluated in their study had not reached saturation even after 3000–4000 hours of exposure at 50°C/85%RH. Similarly, Ardebili et al. [1]

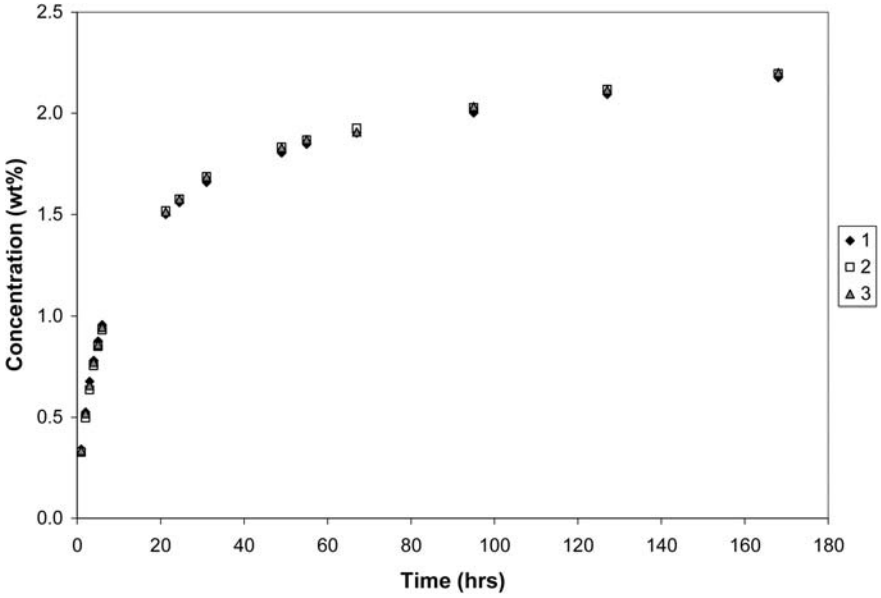

FIGURE 17.1. Moisture uptake profile for UR-A at 85°C/85%RH. (Ferguson and Qu [20], reprinted with permission of ASME.)

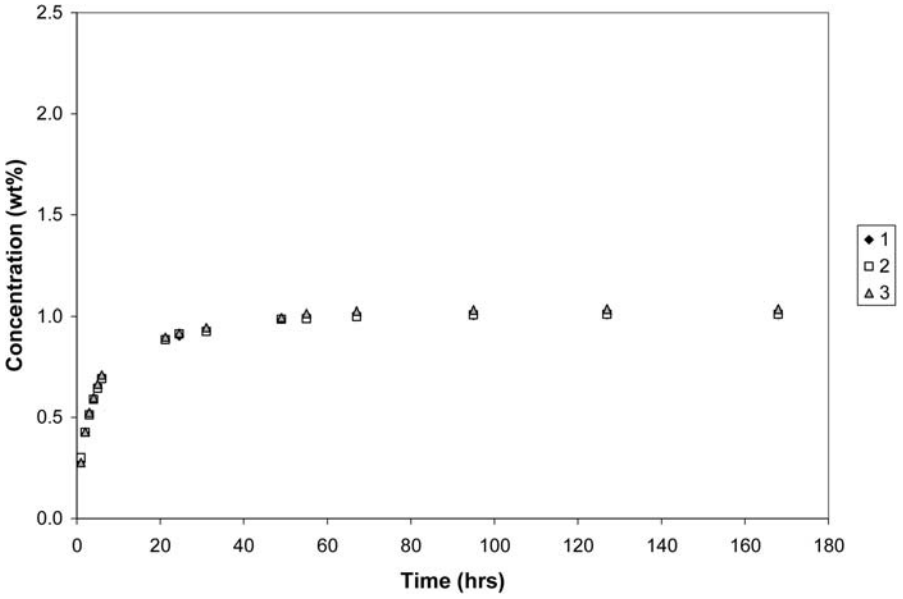

FIGURE 17.2. Moisture uptake profiles for UR-B at 85°C/85%RH. (Ferguson and Qu [20], reprinted with permission of ASME.)

found some of their epoxies to exhibit a gradual increase in moisture content with time, attributing this increase to void growth in the epoxy network caused by swelling.

The diffusivity of moisture through the thickness of the underfill resin is needed to apply an analytical, Fickian solution for modeling the moisture diffusion into the in-

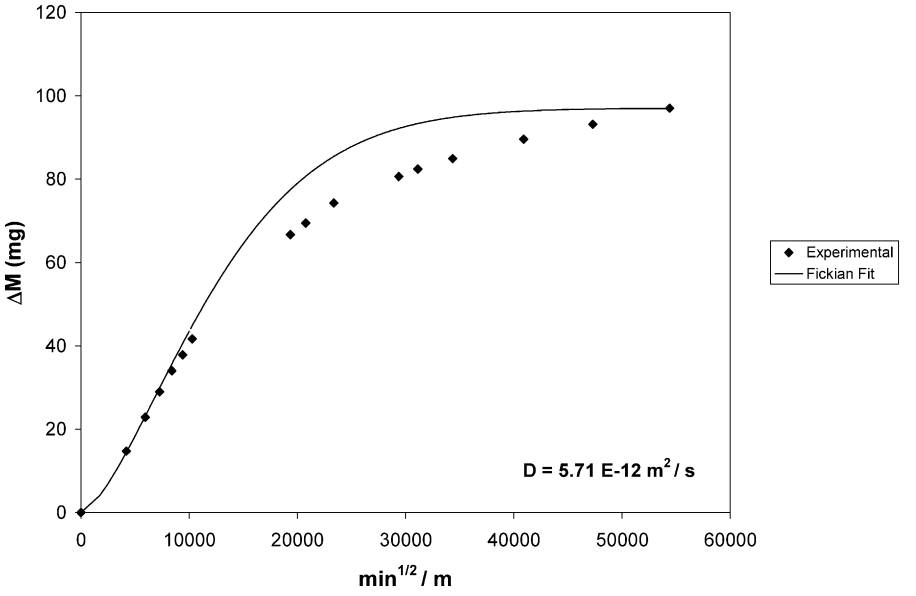

FIGURE 17.3. Fickian curve fit at 85°C/85%RH for UR-A. (Ferguson and Qu [20], reprinted with permission of ASME.)

terfacial fracture test specimens. The diffusion coefficient, D, can be experimentally determined using a test specimen that promotes predominantly one-dimensional diffusion into the test specimen. Using Equation (17.7) with absorption data, the diffusion coefficients were experimentally determined for both UR-A ($D = 5.71E{-}12$ m^2/s) and UR-B ($D = 1.47E{-}11$ m^2/s). Since the diffusion coefficient is a measure of how quickly a material responds to mass concentration changes in its environment, the larger value of diffusivity for UR-B indicates it will respond more quickly to those changes. As a result, UR-B test specimens will approach saturation more rapidly than UR-A test specimens, which quantitatively supports what was already qualitatively observed (Figures 17.1 and 17.2).

A Fickian curve was generated for each underfill to examine the extent that the moisture uptake of the specimens demonstrated Fickian behavior at conditions of 85°C/85%RH. The following relation developed by Shen and Springer [44] was implemented to generate the Fickian profile since it simplifies the infinite series of Equation (17.5):

$$\frac{M_t}{M_\infty} = 1 - \exp\left[-7.3\left(\frac{Dt}{h^2}\right)^{0.75}\right]. \tag{17.8}$$

A Fickian curve for each data set at 85°C/85%RH is shown in Figures 17.3 and 17.4.

It is clear from Figures 17.3 and 17.4 that neither UR-A nor UR-B exhibited true Fickian behavior at 85°C/85%RH, although UR-B appeared to obtain a better curve fit than UR-A. Since test specimens promoted predominately one-dimensional diffusion and exhibited non-Fickian absorption behavior, it is evident that the diffusion coefficients of both UR-A and UR-B were dependent on moisture concentration rather than being constant throughout the entire diffusion process at 85°C/85%RH.

Wong et al. [56] found varied diffusion behavior in the epoxy resins they evaluated at 85°C/85%RH, with some resins exhibiting Fickian diffusion while others did not. They

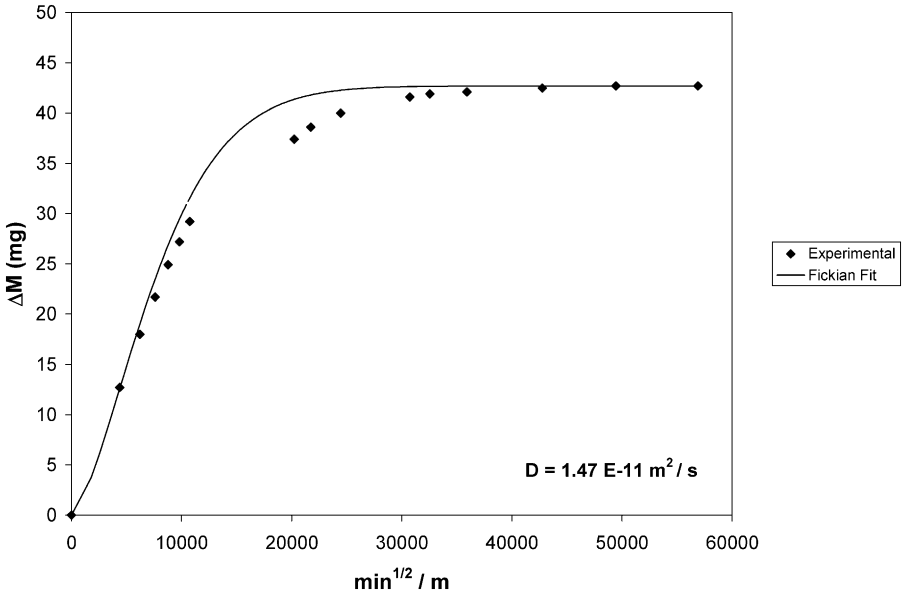

FIGURE 17.4. Fickian curve fit at 85°C/85%RH for UR-B. (Ferguson and Qu [20], reprinted with permission of ASME.)

postulated that diffusivity is constant and moisture diffusion exhibits Fickian behavior for epoxy resins at lower temperature and humidity levels such as 30°C/60%RH. Increasing the humidity level results in a corresponding amplification of the saturation level, while increasing the temperature level produces more prominent non-Fickian behavior [54]. Although test specimens will absorb more moisture in less time at higher temperatures and relative humidity levels, the trade-off is that the specimens will also exhibit an increased likelihood of non-Fickian diffusion behavior. The concentration dependence of the diffusivity in non-Fickian diffusion behavior complicates the modeling of the moisture ingress; however, numerical algorithms have been published that demonstrate how to model the non-Fickian diffusion process [56].

17.2.4. Moisture Absorption Modeling

To illustrate the moisture distribution graphically in interfacial fracture test specimens, a transient, finite element analysis was implemented to model the associated moisture concentration distribution in test specimens for small times of exposure. Since the substrates of the interfacial fracture test specimens were metallic and impermeable to moisture, it should be noted that only the moisture distribution in each underfill was modeled. Results of the finite element model illustrating the transient moisture distribution in the underfill resins are shown in Figures 17.5 and 17.6. Both figures refer to the interfacial fracture test specimens as unmodified, which indicates that this is the moisture absorption behavior exhibited by the test specimens if placed in 85°C/85%RH conditions immediately after test specimen manufacture without consideration to how the moisture uptake could influence fracture results.

It is apparent from the model of the transient moisture ingress that edge effects are significant. This can be clearly seen by examining the interface of the test specimens in

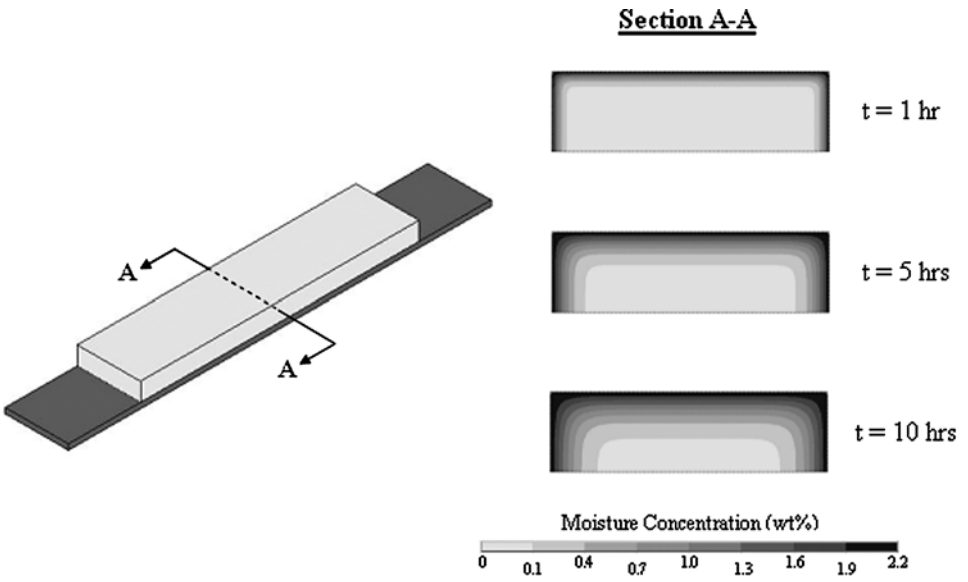

FIGURE 17.5. Moisture concentration distribution for unmodified UR-A interfacial fracture test specimen at 85°C/85%RH after 1, 5, and 10 hours of exposure. (Ferguson and Qu [20], reprinted with permission of ASME.)

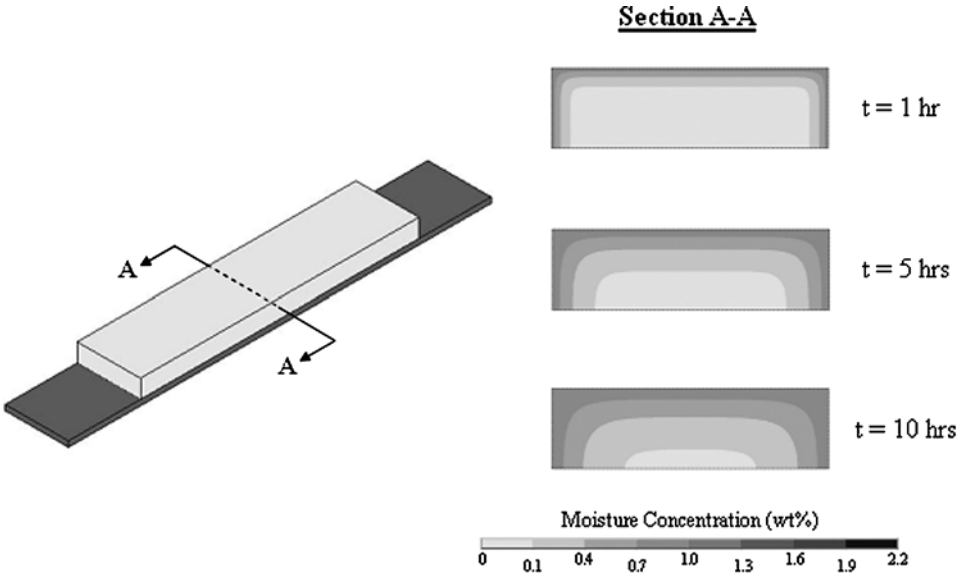

FIGURE 17.6. Moisture concentration distribution for unmodified UR-B interfacial fracture test specimen at 85°C/85%RH after 1, 5, and 10 hours of exposure. (Ferguson and Qu [20], reprinted with permission of ASME.)

Figures 17.5 and 17.6 (bottom of each cross section A–A), where it is evident that a gradient of moisture exists at the interface until saturation is reached. This is undesirable since the interface will experience different levels of moisture spatially relative to the exposure time, which will not allow a fracture toughness measurement to be identified with a par-

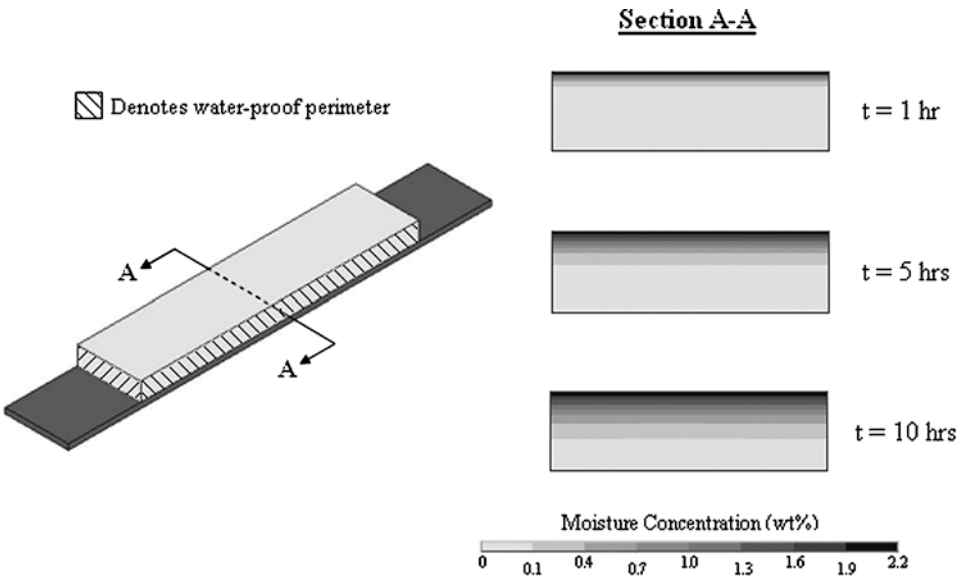

FIGURE 17.7. Moisture concentration distribution for modified UR-A interfacial fracture test specimen at 85°C/85%RH after 1, 5, and 10 hours of exposure.

ticular level of interfacial moisture concentration until saturation is reached. Furthermore, it is also possible that the non-uniform moisture gradient at the interface could influence interfacial fracture toughness results even if saturation is reached in a test specimen. This is attributed to different areas of the interface being exposed to varying degrees of moisture for different periods of time, which could have an effect on fracture toughness results even if test specimens are in a saturated state. Last, wicking of moisture along the interface could also introduce moisture concentration levels that remain unidentified through modeling of the absorption process alone. This would make it difficult to attribute a particular fracture toughness measurement with an associated interfacial moisture concentration level.

In view of these observations, the interfacial fracture test specimen design should be modified with a water-proof perimeter applied to test specimens prior to moisture preconditioning. The application of the water-proof perimeter forces 1D moisture uptake through the top surface of the test specimens and prevents wicking along the interface. Not only does this yield uniform concentrations spatially at the interface, but it also aids in the identification of an interfacial moisture concentration level by utilizing the inherent moisture absorption characteristics of the adhesive to restrict the amount of moisture arriving to the interface. Figures 17.7 and 17.8 depict the moisture concentration distribution in the modified interfacial test specimens.

Although percent weight is dependent on both the specimen volume and density, a comparison between the moisture concentration distributions can be made as a result of both underfills having similar densities (UR-A, $\rho = 1.14 \times 10^{-3}$ g/mm^3 and UR-B, $\rho = 1.16 \times 10^{-3}$ g/mm^3) and volumes. Figures 17.7 and 17.8 illustrate that although UR-A test specimens contain a significantly higher concentration of moisture near the underfill surface, the moisture will actually penetrate the interface first for comparably sized UR-B test specimens. It is clear from the progression of the constant-concentration lines depicted in Figures 17.7 and 17.8 that the moisture traversed much more easily through the UR-B

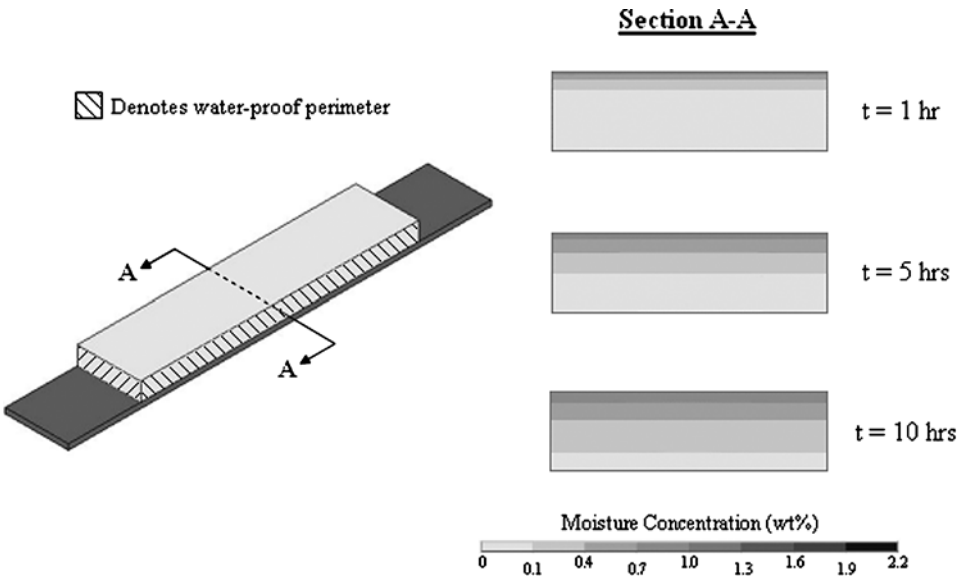

FIGURE 17.8. Moisture concentration distribution for modified UR-B interfacial fracture test specimen at 85°C/85%RH after 1, 5, and 10 hours of exposure.

test specimens. An explanation for this behavior lies in the particular chemistry of each underfill epoxy with respect to the polarity of water molecules. As previously noted, amine functional groups regulate transport through the nanopore channels of the epoxy by either blocking or allowing moisture to traverse the channels depending on the orientation of the resin with respect to nanopore position [48]. UR-A contains amine functional groups, while UR-B is a non-amine containing underfill [20]. Consequently, it would be anticipated that UR-B would have an enhanced diffusion coefficient than UR-A, which was found to be true based on experimental results. As demonstrated in Figures 17.7 and 17.8, the amine functional groups present in UR-A contributed to retard moisture penetration into the amine containing epoxy resin, whereas the moisture diffused more easily through the non-amine epoxy resin, UR-B. From this observation, there are three primary conclusions to consider:

1. Degradation of interfacial adhesion over the entire interface due to the presence of moisture will initially occur in UR-B test specimens prior to comparably sized UR-A test specimens.
2. Further degradation of interfacial adhesion will occur in UR-A test specimens than comparably sized UR-B test specimens for longer exposure times. This is due to UR-A absorbing more aggregate moisture than UR-B at longer durations (Figures 17.1 and 17.2).
3. Amine functional groups present in UR-A retard the rate by which moisture exits the underfill upon redrying. Consequently, UR-A test specimens will take longer to recover the reversible component of adhesion loss upon removal of moisture from the interface than comparably sized UR-B test specimens.

The absorption characteristics, exposure time, and adhesive performance from moisture dictate whether UR-A or UR-B is a more robust product in humid environments. For short exposure times to moist environments and considering only the absorption characteristics, UR-A represents a better encapsulant by retarding the rate of moisture ingress to

the interface through the presence of amine functional groups in its chemistry. Conversely, UR-B represents a better product for longer exposure times to moist environments by absorbing less aggregate moisture than UR-A. Bare in mind neither of the aforementioned statements considers the relative adhesion performance in the presence of moisture nor the extent by which each underfill adhesive bond recovers after multiple exposures to moist environments. These are additional considerations when evaluating the long term reliability of a particular underfill to moist conditions.

17.3. ELASTIC MODULUS VARIATION DUE TO MOISTURE ABSORPTION

The deleterious effect of moisture not only damages interfacial adhesion by being physically present at the interface, but also through the degradation of the elastic modulus of the adhesive and substrate due to moisture uptake. The change in the elastic modulus after moisture uptake can be substantial, which can significantly affect material performance and adhesion results. Consequently, the variation in the elastic modulus of the adhesive and substrate as a function of moisture concentration should be determined to completely characterize the loss in interfacial adhesion due to moisture absorption. Since many of the substrates used in electronic packaging are impermeable to moisture (i.e., copper, aluminum, and silicon), it is often only necessary to characterize the change in the elastic modulus as a function of moisture concentration for the adhesives, which are typically epoxy based and highly susceptible to moisture uptake.

17.3.1. Background

Epoxy adhesives are found in many microelectronic packaging applications and widely used throughout the industry. One of the more substantial developments within the last ten years is underfill, which is an epoxy based encapsulant that mechanically couples the chip to the board. Underfill drastically enhances the fatigue life of microelectronic assemblies when compared to unencapsulated devices [51]; however, since underfills are epoxy based, they are also particularly vulnerable to moisture ingress [20,22,53,56]. Although the absorbed moisture can significantly alter its mechanical performance and the overall microelectronic assembly reliability, very few studies in the electronic packaging literature have addressed the issue of moisture on the mechanical properties of epoxies.

Throughout the literature, the availability of information regarding the effect of moisture on the mechanical properties of epoxy adhesives is in general limited and more work is needed to adequately characterize this response [12,24]. From the work that has been published, it has been found that water absorption can severely modify the mechanical properties of epoxies by decreasing the elastic modulus [36,63], shear modulus [27,64], yield stress [55], and ultimate stress [55] while increasing the failure strain [12,55] as water concentration increases. A representative stress/strain diagram is shown in Figure 17.9 illustrating these effects.

Moisture primarily affects the mechanical properties of epoxy adhesives through three mechanisms: plasticization, crazing, and hydrolysis. The first is considered reversible upon drying, while the latter two are irreversible. Several studies attribute the decrease in modulus due to the plasticizing action of the water on the adhesive [3,12,15,27,49, 55,63,64]. By acting as an external plasticizer to the adhesive, the water spreads the polymer molecules apart and reduces the polymer–polymer chain secondary bonding. This provides more room for the polymer molecules to untangle and move, which results in a softer,

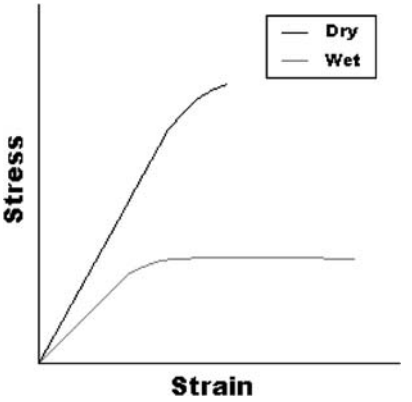

FIGURE 17.9. Representative stress/strain diagram depicting the effect of moisture on the mechanical properties of bulk epoxy adhesives.

more easily deformable mass [42]. Other studies show the decrease in epoxy modulus after moisture absorption resulting from crazing [34,36,37], where the absorbed water can act as a crazing agent continuously decreasing the mechanical strength of epoxies with exposure time in water [34]. This is supported by scanning electron micrographs of epoxies, which show cavities and fractured fibrils that could only be explained by a moisture-induced crazing mechanism [37]. The moisture-induced swelling creates dimensional changes and internal stresses that can ultimately craze and/or crack the material. As a result, lightly cross-linked networks will be more susceptible to crazing than highly cross-linked networks [36]. Last, moisture can also affect the mechanical properties of epoxy adhesives by causing hydrolysis leading to chain scission. Short term exposure to moisture results in chain scission with a chemical addition of water that remains permanently in the epoxy system even after subsequent drying. Long term exposure to moisture can result in an increased probability of chain scission detaching segments from the polymer network, yielding a permanent loss in weight after subsequent drying [59].

Studies by Zanni-Deffarges and Shanahan [63,64] and DeNeve and Shanahan [15] depict the decrease in elastic and shear modulus of an epoxy as a function of time exposure to moisture. Although this information is useful in evaluating the effect of exposure time to moisture on the modulus, it does not depict how the inherent wet modulus values change as a function of concentration. This is due to a gradient of mechanical properties that will exist in the adhesive until saturation is reached, where water concentrations become steady and uniform. Other studies have evaluated the effect of moisture on epoxy adhesives after saturation is established for a given level of moisture preconditioning. These studies have shown a decrease in the elastic modulus of epoxy adhesives of 24% [64], 29% [49], and 86% [49] for saturation concentrations of 4 wt%, 0.9 wt%, and 3.1 wt% respectively; however, they only tested one level of moisture preconditioning to compare to fully dried test results. Consequently, information regarding the mechanical response of epoxy adhesives to different levels of moisture concentrations is incomplete and fundamental insight into the intrinsic response of the adhesives to increasing saturation concentrations of moisture cannot be ascertained.

Even fewer investigations have evaluated the recovery of epoxies upon drying after moisture absorption with little information available regarding the extent of the reversible and irreversible nature of moisture uptake in epoxies. Netravali et al. [38] have shown for

epoxy samples soaked in water at 25°C for 820 hours that much of the loss from moisture results from plasticization and is recoverable upon drying at 30°C for 400 hours; however, samples soaked in water at 70°C for 775 hours were highly irreversible after drying at 70°C for 125 hours. The irreversibility was attributed to water reacting with unreacted epoxide groups. It should be noted that neither groups of samples were completely dry at the time of testing after exposure to water and subsequent drying. Buehler and Seferis [4] found epoxy prepregs soaked in water at 71°C for 1200 hours exhibited varying degrees of reversible and irreversible damage to both the flexural modulus and flexural strength upon drying at 50°C for 450 hours. However, more time was needed to fully dry the specimens in this study as well, with 3% weight concentrations of moisture still existing in the specimens at the time of testing after drying. Wright [57] proposes that the permanent loss of properties that occur due to moisture uptake is most probably due to swelling of the matrix and the production of voids, while Xiao and Shanahan [59] suggest based on absorption behavior that the irreversible damage component of hydrolysis can play a significant role in the degradation process depending on the duration of exposure. Undoubtedly the mechanisms responsible for the observed losses in epoxies from moisture uptake are complex, and the material constitutive damage behavior is not entirely understood.

17.3.2. Effect of Moisture Preconditioning

To help characterize the elastic response of an epoxy adhesive to increasing moisture concentrations, an evaluation of the effect of moisture on the elastic modulus of a no-flow underfill was performed. The particular underfill evaluated was UR-B, which was determined to be ideal for studying the fundamental effect of moisture on interfacial adhesion due to its moisture diffusion kinetics and saturation behavior established from the moisture absorption portion of this research. Flexural specimens were tested in a three-point bend test according to ASTM D790 [2] to determine the effect of moisture on the elastic modulus.

Test specimens were divided into six test groups and subjected to five different levels of moisture preconditioning to ascertain the effect of moisture on the elastic modulus of the underfill. The test groups included fully dry, 85°C only, 85°C/50%RH, 85°C/65%RH, 85°C/85%RH, and 85°C/95%RH, with the latter five test groups being environmentally preconditioned for 168 hours. All test specimens were baked at 115°C for at least 12 hours to remove any moisture that may have been introduced during sample preparation prior to environmental aging, which was performed in a humidity chamber in an atmosphere maintained at a constant temperature (±1°C), humidity (±1%), and pressure (P_{atm}). In addition, all flexural tests were performed with both the surrounding environment and test specimens being at room temperature after environmental preconditioning. No measurable loss in moisture uptake occurred in the test specimens from the time they were removed from the environmental chamber, allowed to cool to room temperature, and experimentally tested.

Figure 17.10 illustrates the effect of moisture preconditioning on the underfill elastic modulus for several different temperature/humidity levels. All moisture preconditioned test specimens were fully saturated at the conclusion of the 168 hour exposure time, hence a gradient of moisture concentration did not occur within the specimens so that the inherent wet modulus was identified. In addition, Differential Scanning Calorimetry (DSC) test results demonstrate that the underfill was fully cured in the flexural specimens for the curing conditions and test specimen size and geometry used [18]. Therefore, incomplete curing

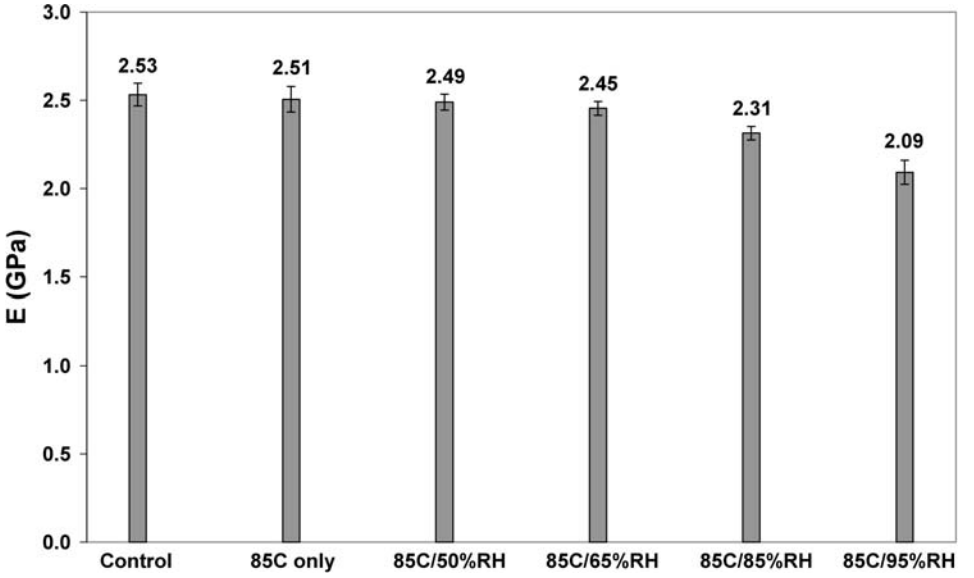

FIGURE 17.10. Effect of moisture preconditioning on the underfill elastic modulus. (Ferguson and Qu [18], reprinted with permission of IEEE.)

of the underfill in the flexural specimens did not influence any observed changes to the elastic modulus of the underfill after moisture preconditioning. Further information on the fundamentals and use of differential scanning calorimetry may be found in the works of Pasztor [40] and Prime [41].

When compared to unaged, control test specimen values, moisture preconditioning at 85°C/50%RH and 85°C/65%RH was found to have little to no effect on the elastic modulus of the underfill. A more noticeable effect occurs at 85°C/85%RH, while conditions of 85°C/95%RH yielded a significant decrease in modulus. To isolate the possible effect of thermal aging at 85°C from moisture preconditioning contributing to the observed changes in the elastic modulus of the underfill, flexural specimens were exposed to conditions of 85°C only for 168 hours and compared to unaged, control test specimen values. As shown in Figure 17.10, thermal aging at 85°C for 168 hours was found to have no effect on the elastic modulus with similar values obtained when compared to the control test group results. Again, it is important to note that all tests were performed at room temperature, hence only the effects of thermal aging were evaluated rather than the effect of testing at elevated temperatures on the elastic modulus. Since all environmental preconditioned test groups were exposed to the same temperature of 85°C and to the same duration of 168 hours, the observed changes in modulus from moisture preconditioning given in Figure 17.10 can be attributed to the effect of moisture and moisture alone.

A summary of the effect of moisture preconditioning on the elastic modulus of the underfill is given in Table 17.1, where C_{sat} represents the saturation concentration of moisture in the test specimens for each respective level of moisture preconditioning and given as both a percent weight change (wt%) and mg H_2O/mm^3.

Since saturation was reached in all moisture preconditioned test specimens prior to removal from the humidity chamber and thermal aging from the 85°C temperature component of moisture preconditioning was found to have no effect on the elastic modulus,

TABLE 17.1.
Change in the underfill elastic modulus from moisture uptake. (Ferguson and Qu [18], reprinted with permission of IEEE.)

T (°C)	RH (%)	C_{sat} (wt%)	C_{sat} (mg H_2O/mm^3)	E (GPa)	Modulus change (%)
Control	—	0	0.0000	2.53 ± 0.06	—
85	50	0.65	0.0075	2.49 ± 0.05	1.6
85	65	0.77	0.0089	2.45 ± 0.04	3.2
85	85	1.02	0.0118	2.31 ± 0.04	8.7
85	95	1.19	0.0138	2.09 ± 0.07	17.4

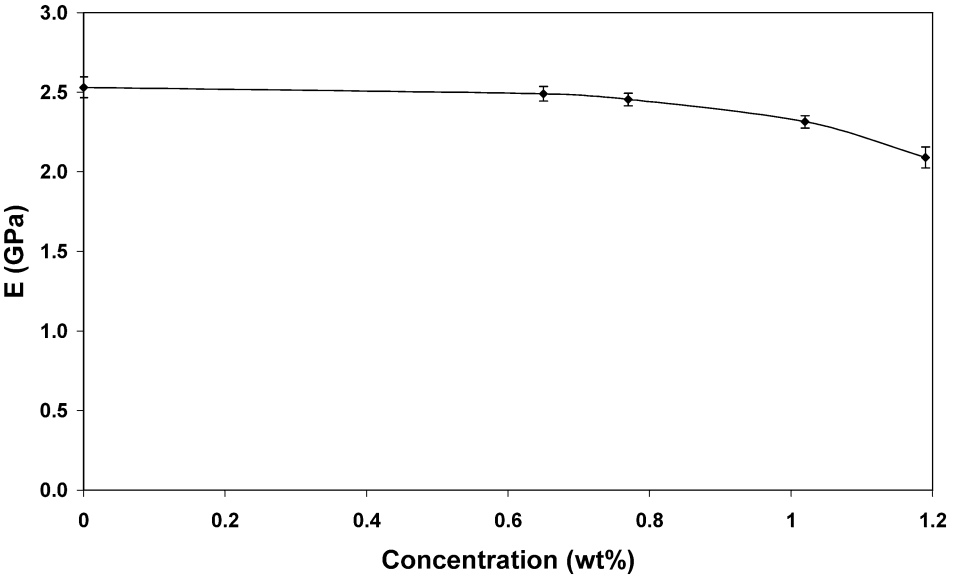

FIGURE 17.11. Underfill elastic modulus variation as a function of moisture concentration (wt%). (Ferguson and Qu [18], reprinted with permission of IEEE.)

the inherent wet modulus was identified and all observed changes in the modulus occurred solely from the influence of moisture. This allows the characterization of the change in modulus of the underfill from moisture uptake as a function of moisture concentration as shown in Figures 17.11 and 17.12.

Figures 17.11 and 17.12 depict the inherent change in the elastic modulus of an epoxy-based adhesive as a function of moisture concentration. Time dependent variation in the elastic modulus after saturation is assumed to be negligible, although it could be a consideration for longer durations of exposure at higher concentrations of moisture as a result of hydrolysis [59]. Previous studies on epoxy adhesives have shown the variation in modulus as a function of the square root of time corrected for specimen thickness [63]; however, this information depicts the change in modulus resulting from a transient, gradient of moisture concentration rather than demonstrating how the inherent wet modulus changes with increasing moisture content. Other studies have identified the inherent wet modulus for a single saturation level and compared to fully dry results [3,49,63]; however, these studies do not show the inherent wet modulus of the same adhesive for several dif-

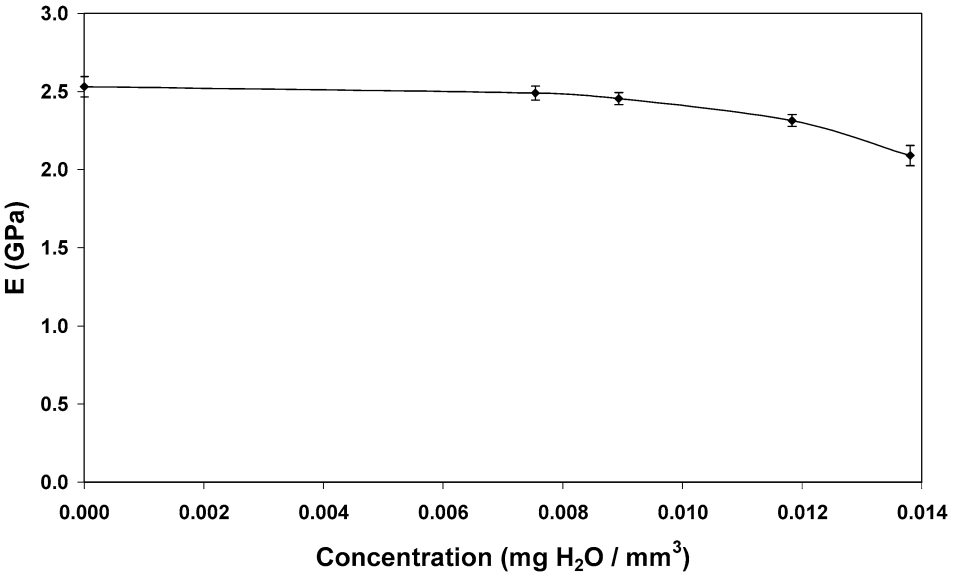

FIGURE 17.12. Underfill elastic modulus variation as a function of moisture concentration (mg H_2O/mm^3). (Ferguson and Qu [18], reprinted with permission of IEEE.)

ferent saturation levels and thus do not show the characteristic response of the adhesive as a function of increasing moisture concentration as given in Figures 17.11 and 17.12. Such information is extremely useful in predictive modeling efforts, where the intrinsic response of the elastic modulus as a function of increasing moisture concentration can be used in a coupled mechanical-diffusion analysis [55] to incorporate the transient effect of the continual variation of elastic modulus as moisture diffuses into the adhesive. These data are not only significant when modeling the effect of moisture on the bulk material behavior, but also on interfacial adhesion, where changes in the mechanical properties of the adhesive due to moisture uptake can play a significant role in the onset of package delamination.

17.3.3. Elastic Modulus Recovery from Moisture Uptake

To further characterize the response of the underfill from moisture uptake and identify the mechanisms responsible for the observed losses in the elastic modulus from moisture absorption, test specimens were moisture preconditioned for 168 hours followed by baking at 95°C until fully dry. A fully dried state was established when there was no measurable change in the weight of a specimen for a period of 24 hours. Since 85°C/85%RH and 85°C/95%RH moisture preconditioning conditions were found to noticeably decrease the elastic modulus of the underfill, only those conditions were evaluated for recovery of the elastic modulus from moisture uptake upon redrying. Figure 17.13 provides a graphical depiction of the recovery results for the underfill elastic modulus.

As shown in Figure 17.13, much of the observed loss in the elastic modulus from moisture uptake was recoverable upon subsequent drying. Since plasticization is the only primary degradation mechanism attributed to moisture that is regarded as a reversible process, the recovery results demonstrate that the majority of the loss in modulus resulted from plasticization of the underfill from moisture uptake. To further evaluate the change

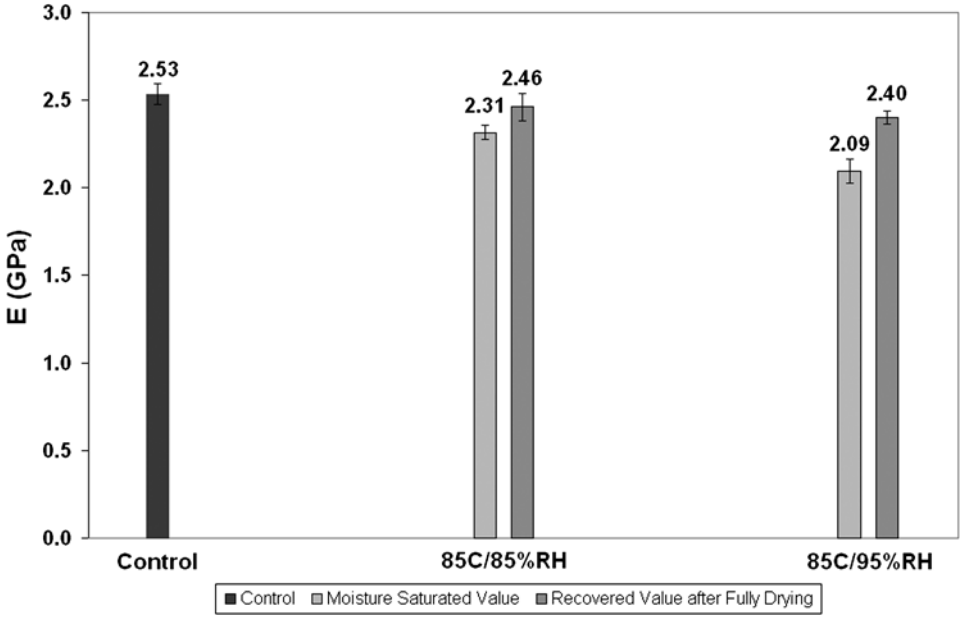

FIGURE 17.13. Recovery of the underfill elastic modulus on removal of moisture. (Ferguson and Qu [18], reprinted with permission of IEEE.)

TABLE 17.2.
Recoverability of the underfill elastic modulus from moisture uptake after subsequent drying. (Ferguson and Qu [18], reprinted with permission of IEEE.)

T (°C)	RH (%)	C_{sat} (wt%)	E_{sat} (GPa)	$E_{recovery}$ (GPa)	*Recoverability* (%)
Control	—	0.00	2.53 ± 0.06	—	—
85	50	0.65	2.49 ± 0.05	—	—
85	65	0.77	2.45 ± 0.04	—	—
85	85	1.02	2.31 ± 0.04	2.46 ± 0.08	68.2
85	95	1.19	2.09 ± 0.07	2.40 ± 0.05	70.5

in elastic modulus from moisture uptake, the recoverability for the elastic modulus will be defined as follows:

$$\textit{Recoverability}\ (\%) = \frac{E_{recovery} - E_{sat}}{E_{dry} - E_{sat}} \cdot 100, \tag{17.9}$$

where $E_{recovery}$ is the value of the elastic modulus upon fully drying from the moisture saturated state, E_{sat} is the saturated value of the elastic modulus after moisture absorption, and E_{dry} is the unaged, control value of the elastic modulus. The recoverability of the elastic modulus is given in Table 17.2.

Although a significant portion of the elastic modulus was recoverable after fully drying, some irreversible, permanent damage did occur. The average recoverable value of the elastic modulus suggests slightly more irreversible damage occurred at higher humidity levels, but it cannot be concluded unequivocally solely based on the modulus results due

to the uncertainty associated within the two measurements. However, it can be concluded when considering the results from moisture uptake data. After fully drying, there was a slight net permanent weight increase in the test specimens, with specimens moisture preconditioned at 85°C/85%RH retaining $1.3 \pm 0.5\%$ of the total absorbed water while specimens moisture preconditioned at 85°C/95%RH retaining $2.3 \pm 0.4\%$ of the total absorbed water. The permanent weight increase in the test specimens after subsequent fully drying suggests that at least part of the irreversible damage resulted from hydrolysis with a greater extent occurring at higher humidity levels. In addition to hydrolysis, it is also possible that moisture-induced crazing also contributed to the irreversible damage to the elastic modulus. Overall, the irreversible damage was small with the majority of the loss in the elastic modulus from moisture uptake being fully recoverable after subsequent drying.

17.4. EFFECT OF MOISTURE ON INTERFACIAL ADHESION

The effect of moisture on interfacial adhesion is governed by two fundamental mechanisms. The first is the rate at which moisture is delivered to the interface, and the second is the change in adhesion performance as a consequence of moisture being present in the adhesive structure. This includes not only the primary effect of moisture being directly present at the interface itself, but also the secondary effect of moisture altering the mechanical performance of the two materials that constitute the bimaterial interface. Having previously quantified both the rate at which moisture is delivered to the interface and the degrading effect of moisture on the elastic modulus of the materials that constitute the bimaterial interface, a model depicting the intrinsic change in interfacial adhesion as a function of moisture concentration is developed. Interfacial fracture mechanics is used to characterize this change to develop relationships that are independent of test specimen geometry.

17.4.1. Background

With interconnect density increasing and package size decreasing, several adaptations to microelectronic assemblies have been developed to accommodate the increasing demand in both cost and performance requirements. In particular, epoxy-based encapsulants have been extensively used in microelectronic devices to enhance package reliability, provide environmental protection, and improve manufacturing yields. To insure these benefits are not compromised, the structural integrity of the adhesive bond must be maintained. Characterizing the primary adhesion mechanisms and identifying the factors that affect the strength and durability of encapsulants are critical to their success.

Traditional encapsulation processes, such as transfer molding, cavity filling, and glob-topping, are used to protect the IC device from environmental pollutants and provide mechanical support. In these devices, copper alloys are typically used as a lead frame material due to their low cost in conjunction with their high electrical and thermal conductivity. However, the adhesion at the epoxy/copper interface is poor [7,9,29,32]. In addition, the copper surface is highly susceptible to oxidation. This is an additional consideration when evaluating the interfacial adhesion of adhesives with copper.

A more recent encapsulant developed within the last ten years is underfill, which is an epoxy-based encapsulant that mechanically couples the chip to the board. Underfill drastically enhances the fatigue life of microelectronic assembles when compared to unencapsulated devices [51], provided the adhesive bond between the underfill and the printed

wiring board, solder mask, copper, silicon, passivation, and solder is maintained. Characterizing the adhesion of underfill to these substrates has been the focus of several studies in adhesion and reliability research [13,14,17,19,60].

Although epoxy encapsulants have many benefits, they are susceptible to moisture uptake. A typical epoxy formulation can absorb between 1 and 7 wt% moisture [47], which can have a detrimental effect on interfacial adhesion and drastically reduce the reliability of encapsulated devices. While it has been shown that moisture can significantly alter adhesive performance in microelectronic packaging [21,34], the interfacial and material constitutive damage behavior from moisture exposure is not well understood. This largely arises due to the difficulty of the problem, which is governed by two fundamental mechanisms. The first is the rate at which moisture is delivered to the interface. The second is the response of the interfacial adhesion to varying levels of moisture concentration, where the deleterious effect of moisture not only affects interfacial adhesion by being physically present at the interface, but also through the degradation of the mechanical properties of the epoxy adhesive due to moisture uptake. Mass transport and in particular the diffusion of moisture in epoxy adhesives has been studied by several sources and is fairly well established [47,48, 52,54,56]; however, the response of interfacial adhesion to moisture is much less understood. Although several studies have addressed the issue of moisture, much more work needs to be completed and there currently exists a lag in fundamental empirical data depicting the loss in interfacial adhesion as a function of interfacial moisture concentration. Since there exists this lag in experimental data, even less effort has been spent on developing predictive models that account for the effect of moisture on interfacial adhesion.

Of particular interest to the long-term reliability of an adhesive bond is ascertaining the permanent damage to the bond from exposure to moisture. Very few studies have examined the reversible and irreversible components of the loss in adhesion from moisture after subsequent drying. This has significant practical aspects, as the recoverability of the interface from moisture will identify the severity of the moisture damage. If the loss in adhesion from moisture is largely unrecoverable and irreversible, then the service life of the adhesive joint will be severely, permanently compromised as a result of exposure to moisture. Such consequences would bring added emphasis to protecting the encapsulated package from moisture ingress and developing more robust, moisture-resistant adhesives.

When evaluating the moisture recovery of an adhesive joint, there are two aspects to consider. The first is the recovery of the materials that constitute the adhesive joint, as absorbed moisture can alter the mechanical performance of those materials and indirectly affect adhesion [18]. The second aspect is the recovery of the interfacial bonding itself, as the direct presence of moisture at the interface can significantly alter adhesion. Butkus [5] examined the permanent change in Mode I fracture toughness of Aluminum/FM73M/Aluminum and Aluminum/FM73M/Boron-Epoxy joints after 5000 hours at 71°C and $>$90%RH followed by 5000 hours of desiccation at 22°C/10%RH prior to testing. Both the Al/FM73M/Al joints and the Al/FM73M/Boron-Epoxy joints recovered very little of their fracture toughness on subsequent drying, demonstrating large, permanent losses in toughness after exposure to moisture. Orman and Kerr [39] have shown that although some of the strength lost in the epoxy-bonded aluminum joints they studied was recovered, there was noticeable permanent damage from moisture suggesting an irreversible disruption at the interface as a result of attack by water. Contrary to this claim, Shaw et al. [43] found that nearly all of the strength lost after immersing steel/epoxy lap shear joints in distilled water for three weeks was recovered after drying. They attributed the loss in strength after moisture preconditioning to plasticization of the epoxy adhesive,

which is generally regarded as a reversible process. Dodiuk et al. [16] found exposure to moisture of their epoxy/aluminum joints caused a reduction in lap shear strength; however, if the moisture concentration was below 0.3 wt%, the strength was fully recoverable after drying indicating a completely reversible process. The authors gave no explanation to this observed behavior other than to state that moisture concentrations exceeding 0.3 wt% would result in an irreversible process and permanent loss of adhesion at the interface. Undoubtedly the mechanisms responsible for the observed losses in both material behavior and interfacial adhesion from moisture uptake are complex, and the material constitutive damage behavior is not entirely understood.

17.4.2. Interfacial Fracture Testing

Interfacial fracture toughness is defined as the critical value of the energy release rate, G_c, at which a bimaterial interface will begin to delaminate. It is a property that characterizes the adhesion of a bimaterial interface, independent of the size and geometry of the cracked body. For a bimaterial interface loaded in four point bending under plane strain conditions, it can be shown that the critical value of the energy release rate, G_c, can be determined using the following equation [26]:

$$G = \frac{1}{2\overline{E_1}}\left(\frac{12M^2}{h^3}\right) - \frac{1}{2\overline{E_2}}\left(\frac{M^2}{Ih^3}\right), \tag{17.10}$$

where

$$\overline{E_i} \equiv \frac{E_i}{1-\nu_i^2}, \tag{17.11}$$

M is the moment, ν is Poisson's ratio, E is the elastic modulus, subscript 1 refers to material 1, subscript 2 refers to material 2, h is the height of material 1, and I is the dimensionless moment of inertia.

Since the interfacial fracture toughness only specifies the magnitude of the crack tip singularity, the mode mixity, ψ, must be determined from the complex stress intensity factor K. For a two-dimensional system, the complex stress intensity factor, K, is given by:

$$K = K_1 + iK_2. \tag{17.12}$$

For four-point loading conditions it can be shown [26]:

$$K = h^{-i\varepsilon}\sqrt{\frac{1-\alpha}{1-\beta^2}}\left(\frac{P}{\sqrt{2hU}} - ie^{i\gamma}\frac{M}{\sqrt{2h^3V}}\right)e^{i\omega} \tag{17.13}$$

with the mode mixity given by:

$$(K_1 + iK_2)L^{i\varepsilon} = |(K_1 + iK_2)|e^{i\psi}, \tag{17.14}$$

$$\psi = \tan^{-1}\left(\frac{\mathrm{Im}(KL^{i\varepsilon})}{\mathrm{Re}(KL^{i\varepsilon})}\right), \tag{17.15}$$

where L is the characteristic length and ε is a dimensionless quantity given by Hutchinson and Suo [26]. As shown in Equation (17.15), the mode mixity for a test specimen requires the specification of some length quantity, L. The choice for L is arbitrary, but it should be selected as a fixed length and reported with the calculated values for the mode mixity.

The flexural beam test for interfacial fracture testing has three primary benefits. First, it yields intermediate values for mode mixity, which is representative of the values experienced by electronic devices during actual application. Second, it provides a means for successful interfacial fracture test specimen construction utilizing substrates and adhesives common to microelectronic packaging. Last, the flexural beam test configuration yields an open-faced test specimen design, which allows saturated, steady state conditions to be reached in the test specimens in a relatively short amount of time. This is due to the large surface area for moisture uptake relative to the short diffusion path to the interface.

17.4.3. Effect of Moisture Preconditioning on Adhesion

Interfacial fracture mechanics was used to characterize the intrinsic effect of moisture on adhesion. The adhesive used was an epoxy-based underfill developed for no-flow assembly, designated as UR-B in this research. This particular underfill was determined to be ideal for studying the fundamental effect of moisture on interfacial adhesion due to its moisture diffusion kinetics and saturation behavior established from the moisture absorption portion of this research. The substrate used was oxygen-free electronic grade copper, alloy 101. The copper substrates were polished to a mirror finish and cleaned using the routine procedure given by Shi and Wong [45] prior to bonding. This was done to isolate the intrinsic effect of moisture on adhesion without mechanical interlocking and/or surface contamination influencing the results. Symmetric interface cracks were introduced into the underfill/copper bilayer test specimens by using a molding compound release agent [19]. Based on the results from the moisture absorption analysis, a water-proof perimeter was applied to the interfacial fracture test specimens during moisture preconditioning and removed before fracture testing. This perimeter served two purposes. First, the application of the perimeter forced 1D diffusion through the top, open surface of the underfill, yielding uniform concentrations of moisture spatially across the entire interface for the full duration of exposure to the humid preconditioning environment. Second, the water-proof perimeter prevented moisture wicking at the interface, which allowed identification of the test specimen moisture concentration by utilizing the inherent moisture absorption characteristics of the adhesive. Completed specimens were tested in a four-point bend test at room temperature to measure the critical load of fracture for the interface. A completed representative interfacial fracture toughness test specimen is shown in Figure 17.14.

Test specimens were divided into five test groups and subjected to four different levels of moisture preconditioning to ascertain the effect of moisture on interfacial fracture toughness. The test groups included fully dry, 85°C only, 85°C/50%RH, 85°C/65%RH, and 85°C/85%RH, with the latter four test groups being environmentally preconditioned for 168 hours. The 85°C temperature component in each moisture preconditioning environment will enhance diffusion rates and drive more moisture into test specimens over a smaller timeframe. In addition, as temperature increases, the moisture capacity of air increases. Consequently, more moisture will be available to diffuse into test specimens at higher relative humidity levels compared to similar, high relative humidity levels at lower temperatures. By gradually increasing the relative humidity while maintaining the temperature constant, the change in interfacial fracture toughness as a function of increasing

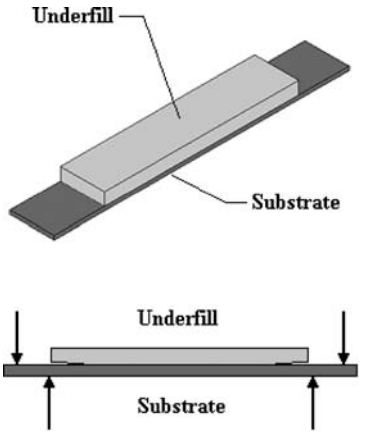

FIGURE 17.14. Interfacial fracture toughness test specimen.

moisture content can be identified. For additional information on psychometrics, refer to Thermodynamics: An Engineering Approach by Cengel and Boles [6].

All test specimens were baked at 115°C for at least 12 hours to remove any moisture that may have been introduced during sample preparation prior to environmental aging, which was performed in a humidity chamber in an atmosphere maintained at a constant temperature (±1°C), humidity (±1%), and pressure (P_{atm}). All interface fracture tests were performed with both the surrounding environment and test specimens being at room temperature after environmental preconditioning. No measurable loss in moisture uptake occurred in the test specimens from the time they were removed from the environmental chamber, allowed to cool to room temperature, and experimentally tested.

Using the experimentally measured value for the critical load of fracture in conjunction with previously identified elastic modulus results, the interfacial fracture toughness of the underfill/copper test specimens was determined using Equation (17.10) for each particular level of moisture preconditioning. Figure 17.15 provides a graphical depiction of the results depicting the effect of environmental preconditioning on the underfill/copper interfacial fracture toughness.

The entire range of mode mixity for all interfacial test specimens fell between −37.41° to −37.64°. The substrate height was used to define the characteristic length for all reported toughness values when evaluating the mode mixity. Since the variation in mode mixity was negligible, the effect of this variation affecting interfacial fracture toughness results between different test groups is insignificant. Consequently, interfacial fracture toughness results for different moisture preconditioned test groups can be compared to one another to ascertain the effect of increasing moisture content on toughness values. In addition, saturation was reached in each moisture preconditioning environment prior to fracture testing. As a result, a gradient of moisture concentration did not exist in the interfacial fracture toughness test specimens during testing. As shown in Figure 17.15, it is clear that the contribution of thermal aging at 85°C did not significantly affect the interfacial fracture toughness of the underfill/copper interface. It is important to remember that all tests were performed at room temperature, hence only the effects of thermal aging were evaluated rather than the effect of testing at elevated temperatures. Since all environmental preconditioned test groups were exposed to the same temperature component of 85°C and duration of 168 hours, any observed changes in the fracture toughness after

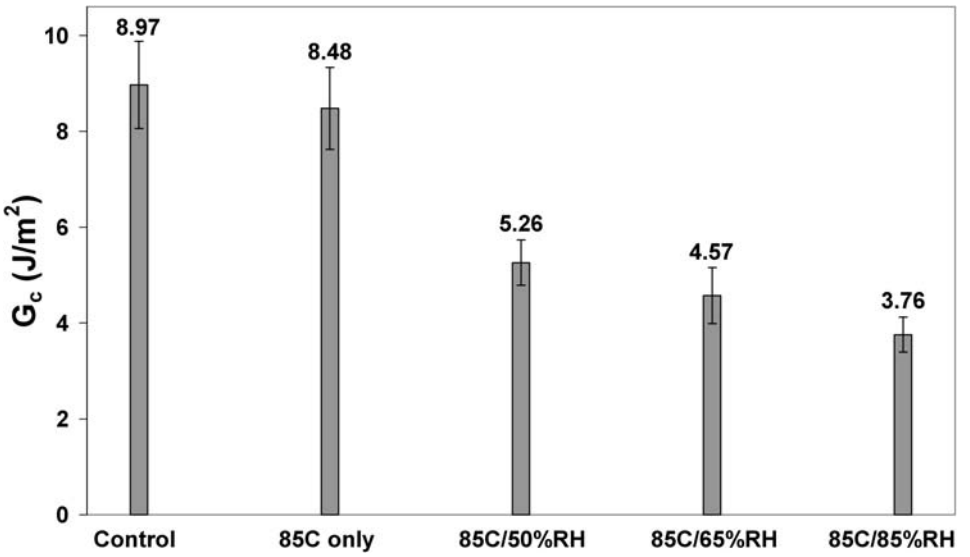

FIGURE 17.15. Effect of environmental preconditioning on the interfacial fracture toughness of the underfill/copper interface.

TABLE 17.3.
Change in the underfill/copper test specimen interfacial fracture toughness from moisture uptake.

T (°C)	RH (%)	C_{sat} (wt%)	C_{sat} (mg H_2O/mm^3)	G_c (J/m^2)	Toughness change (%)
Control	—	0	0.0000	8.97 ± 0.91	—
85	50	0.65	0.0075	5.26 ± 0.47	41.4
85	65	0.77	0.0089	4.57 ± 0.58	49.1
85	85	1.02	0.0118	3.76 ± 0.36	58.1

moisture preconditioning can be attributed to the contribution of moisture. Moisture preconditioning at 85°C/50%RH, 85°C/65%RH, and 85°C/85%RH had a substantial effect on the interfacial fracture toughness and yielded decreases of 41.4%, 49.1%, and 58.1% respectively. A summary of the effect of moisture preconditioning on the interfacial fracture toughness is provided in Table 17.3, where C_{sat} represents the saturation concentration of moisture for each respective level of moisture preconditioning and given as a percent weight change (wt%).

Figures 17.16 and 17.17 depict the inherent change in the underfill/copper interfacial fracture toughness as a function of moisture concentration.

Based on Figures 17.16 and 17.17, it is clear that the change in the interfacial fracture toughness is sensitive to small amounts of moisture. A significant reduction in interfacial adhesion was observed for concentrations as low as 0.65 wt%. Since the moisture did not significantly alter the elastic modulus of the underfill adhesive for the moisture conditions evaluated for the interfacial fracture toughness, plasticization of the underfill from moisture contributed little to the change in the interfacial fracture toughness. As a result, the reduction in toughness is primarily attributed to the weakening of the underfill/copper interface due to the direct presence of moisture at the interface. The moisture at the interface could decrease the adhesion through displacement of the underfill reducing Van der Waals forces

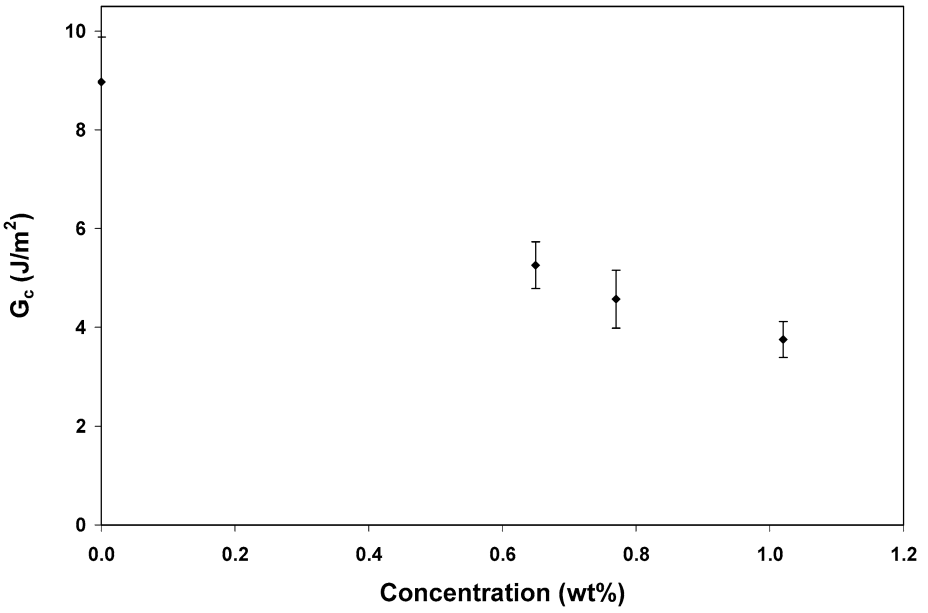

FIGURE 17.16. Underfill/copper interfacial fracture toughness variation as a function of moisture concentration (wt%).

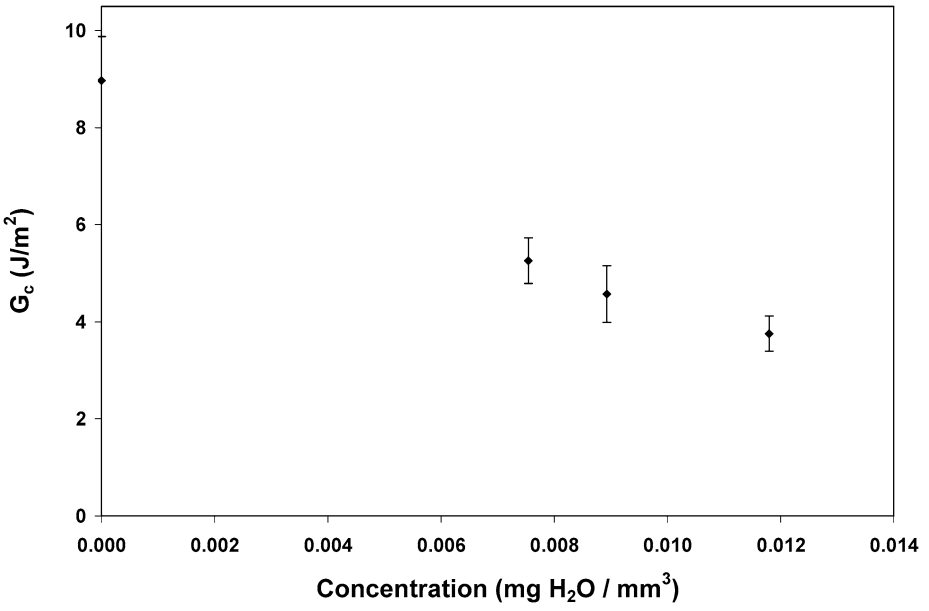

FIGURE 17.17. Underfill/copper interfacial fracture toughness variation as a function of moisture concentration (mg H_2O/mm^3).

as well as possible chemical degradation of adhesive bonds. Further investigations into the exact failure mechanism from moisture at the interface are provided in detail in subsequent sections of this chapter.

17.4.3.1. Moisture Induced Swelling In addition to the mechanical load applied to test specimens during interfacial fracture testing, the interface is also subjected to hygro-swelling and thermal contraction mismatch effects between the adhesive and substrate. These two effects have opposite outcomes on the interface, as the contribution from the hygro-swelling mismatch will cause the underfill to be in compression, while the contribution from the thermal contraction mismatch will cause the underfill to be in tension. This is attributed to the different stress free environments for each case. For the case of the hygro-swelling mismatch, fully dry conditions represent a stress-free state for the interface. As moisture is absorbed in the underfill, it will cause the underfill to expand, while the moisture impermeable substrate will retain its original dimensions. Since the moisture expansion in the underfill will be constrained by the substrate, the expansion in the underfill will yield compressive stresses within the underfill. For the case of the thermal contraction mismatch, the curing temperature of the underfill represents a stress-free state for the interface. Once test specimens are removed from the oven and allowed to cool to room temperature, the thermal mismatch between the copper and the underfill will cause the underfill to be in tension due to it wanting to shrink more than the copper substrate (CTE of experimental materials: underfill = 75 ppm/°C, copper = 17 ppm/°C). Whether the interface is dominated by the hygro-swelling mismatch, thermal contraction mismatch, or possibly neither due to the effects of one another canceling each other out for a particular moisture saturation level will depend on the characteristics of the materials that constitute each bimaterial interface relative to their moisture preconditioning environment.

To investigate the effect of hygro-swelling on interfacial fracture test results, the moisture swelling coefficient, β, of the underfill was experimentally determined for each moisture preconditioning environment. The moisture swelling coefficient is defined as

$$\beta = \frac{\Delta\ell/\ell_o}{C_{sat}}, \tag{17.16}$$

where $\Delta\ell$ is the change in length of the specimen due to moisture absorption, ℓ_o is the initial dry length of the specimen, and C_{sat} is the saturation moisture concentration. Using Equation (17.16) with experimental test data, the moisture swelling coefficient was determined for conditions of 85°C/50%RH ($\beta = 1987$ ppm/wt%), 85°C/65%RH ($\beta = 1907$ ppm/wt%), 85°C/85%RH ($\beta = 1808$ ppm/wt%). Having identified the moisture swelling coefficient for each moisture preconditioning environment, a comparison can be made between the hygro-swelling and thermal mismatch strains for the underfill/copper interface. The hygro-swelling mismatch strain, ε_h, and thermal mismatch strain, ε_t, are defined as follows:

$$\varepsilon_h = \beta_1 C_{sat,1} - \beta_2 C_{sat,2}, \tag{17.17}$$

$$\varepsilon_t = (\alpha_1 - \alpha_2)(T_f - T_i), \tag{17.18}$$

where β is the moisture swelling coefficient, C_{sat} is the equilibrium moisture saturation concentration, α is the coefficient of thermal expansion, T is the temperature, and subscripts 1 and 2 refer to the two materials that constitute the bimaterial interface. The hygro-swelling mismatch strain and thermal expansion mismatch strain were calculated using Equations (17.17) and (17.18) respectively for each moisture preconditioning environment. Since the cooling of the interfacial fracture test specimens from the cure temperature to

TABLE 17.4.
Comparison of hygro-swelling and thermal mismatch strains for the underfill/copper interfacial fracture test specimens.

Environment	β (ppm/wt%)	C_{sat} (wt%)	ε_h	α_{uf} (ppm/°C)	α_{Cu} (ppm/°C)	T_i (°C)	T_f (°C)	ε_t
85°C/50%RH	1987	0.65	0.0013	75	17	190	25	0.0096
85°C/65%RH	1907	0.77	0.0015	75	17	190	25	0.0096
85°C/85%RH	1808	1.02	0.0018	75	17	190	25	0.0096

room temperature will result in a thermal contraction, while the uptake of moisture will result in an expansion from swelling, it should be noted that the hygro-swelling and thermal expansion mismatch strains act in opposite directions. The results are given in Table 17.4.

As shown in Table 17.4, the thermal mismatch strains were significantly greater than the hygro-swelling mismatch strains for all moisture preconditioning environments by roughly an order of magnitude. It is clear that the thermal mismatch strain dominated the interaction at the interface and was only slightly offset by a small contribution from the hygro-swelling mismatch strain for this particular bimaterial interface. As a result, the underfill will be in tension during interfacial fracture testing, effectively preloading the interface and requiring a lower critical load of fracture, P_c, from mechanical testing to advance the interface crack. Consequently, interfacial fracture toughness values will represent a conservative estimate of the interfacial fracture toughness of the interface. In addition, it is clear that increasing the saturation concentration did not significantly increase the hygro-swelling mismatch strain. All interfaces for all environments experienced similar hygro-swelling mismatch strains for the materials and moisture preconditioning environments tested in this study. Consequently, the trends exhibited in the interfacial fracture toughness as moisture concentration increases are essentially independent of the hygro-swelling mismatch relative to one another, and the observed changes between the different moisture preconditioning environments can be predominately attributed to more moisture being present at the interface resulting in a greater loss of adhesion.

17.4.3.2. Interfacial Hydrophobicity The polarity of the water molecule will affect its behavior at the interface, which can influence the extent of environmental degradation of an adhesive joint due to the presence of moisture [33]. The polar behavior of water arises from its structure, which is composed of a single oxygen atom bonded to two hydrogen atoms. The hydrogen atoms are covalently bonded to the oxygen atom through shared electrons. Two pairs of electrons surrounding the oxygen atom are involved in covalent bonds with hydrogen; however, there are also two unshared pairs of electrons (lone-pair) on the other side of the oxygen atom, which shift the electron cloud of the water molecule over to the oxygen atom as shown in Figure 17.18.

This uneven distribution of electron density in the water molecule yields a partial negative charge (δ^-) on the oxygen atom and a partial positive charge (δ^+) on the hydrogen atoms, giving rise to the polarity of the water molecule. Polarity allows water molecules to bond with each other, and hydrogen bonds will form between two oppositely charged ends of a water molecule as shown in Figure 17.19.

The hydrogen bonds have about a tenth of the strength of an average covalent bond, and are being constantly broken and reformed in liquid water. The polarity will also allow water to molecules to bond with other polar molecules, which will affect how the water will wet on different surfaces. Surfaces that contain polar molecules are hydrophilic. They

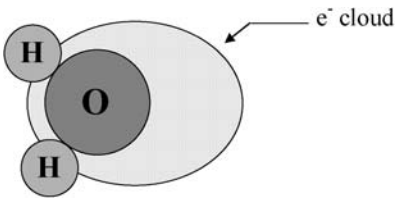

FIGURE 17.18. Electron cloud distribution on a water molecule.

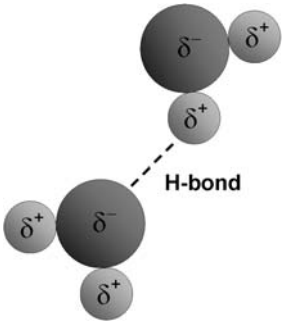

FIGURE 17.19. Hydrogen bonding between water molecules.

interact with the water molecules to enhance wetting, causing the water to smear flat. If a surface contains alcohols, O, or N, it will probably be hydrophilic. Conversely, surfaces that contain nonpolar substances are hydrophobic. They cannot interact with the water molecules, causing it to form a bubble on the surface. In general, if a surface contains C, H, or F, it will probably be hydrophobic.

Most materials will not be purely hydrophobic or hydrophilic, but will have varying degrees to which they are considered one or the other. This is addressed in Hydrophobicity, which is the study of the wetting characteristics of water on surfaces. One method used to test the hydrophobicity of a surface is through measurement of the contact angle, θ, using water as the probe liquid. The contact angle represents a balance between the adhesive forces between the liquid and solid and cohesive forces in the liquid. The adhesive forces cause the liquid drop to spread, while the cohesive forces cause the liquid drop to retain the shape of a sphere. The contact angle is a direct measure of wettability and provides an effective means to evaluate many surface properties such as surface contamination, surface hydrophobicity, surface energetics, and surface heterogeneity. When $\theta > 0$, the liquid is nonspreading and reaches an equilibrium position between the liquid-fluid and solid-liquid interfaces. When $\theta = 0$ the liquid wets without limit and spontaneously spreads freely over the surface. Hydrophobic surfaces repel water and produce high contact angles. Hydrophilic surfaces attract water and produce low contact angles. Figure 17.20 illustrates the contact angle behavior of water on both hydrophobic and hydrophilic surfaces.

By utilizing water as the probe liquid, the interfacial hydrophobicity can be ascertained by measuring the water contact angle of both the adhesive and substrate. To determine the hydrophobicity of interfacial fracture test specimens, contact angle measurements were made for the adhesive and substrate evaluated in this study. Both the clean copper substrate and underfill adhesive exhibited fairly hydrophobic behavior with contact angles of 74° and 83° respectively. Having established the hydrophobicity of the substrate

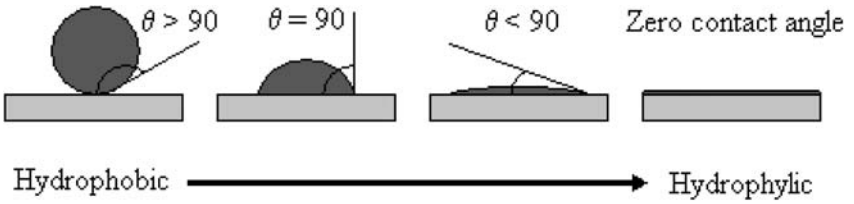

FIGURE 17.20. Hydrophobic and hydrophilic water contact angle behavior.

and adhesive, the interfacial hydrophobicity of the underfill/copper interfacial fracture test specimens can be evaluated. When addressing the relative hydrophobicity of the substrate and adhesive to moisture behavior at the interface, the interaction can become complex. The surface with the most dominant degree of hydrophobicity will govern the shape and response of the water at the interface. For example, if a hydrophobic substrate is bonded with a hydrophilic adhesive, then the water at the interface will want to minimize contact with the substrate and maximize contact with the adhesive. Depending on imperfections in the bonding, surface roughness, and the relative degree of hydrophobicity of the substrate to the adhesive, water at the interface will more or less form a somewhat hemi-spherical shape at the interface, with the spherical end minimizing contact on the substrate and the open end maximizing contact on the adhesive. Naturally, the shape of the water at the interface can have various permutations of the aforementioned shape depending on the degree of hydrophobic behavior of the substrate relative to the hydrophilic behavior of the adhesive, but the general idea remains the same. For other systems with varying degrees of hydrophobicity, the shape of the water at the interface relative to the hydrophobicity of the substrate and adhesive can be extremely difficult to characterize; however, qualitative conclusions can be made. For the case of the underfill/copper interfacial fracture test specimens, the relative hydrophobicity of the adhesive to the substrate was similar; consequently, the wetting behavior of the moisture at the interface would not be significantly dominated by either the adhesive or substrate.

An additional consideration unique to environmental preconditioning is the growth of oxides affecting the interfacial hydrophobicity. Copper has a strong affinity to oxygen, and the development of an oxidation layer between the substrate and adhesive after bonding is inevitable. Initially, cuprous oxide, Cu_2O, will form followed by the formation of a layer of cupric oxide, CuO. The oxidation of copper substrates can be significant, and previous studies have shown that the water contact angle on copper is affected by oxidation [7,25, 28,61]. Due to oxidation growth on the copper substrates, contact angle measurements were made for each preconditioning environment to monitor any change in the hydrophobicity of the copper surface.

Since the copper bonding surface of the interfacial fracture test specimen will be shielded by the underfill adhesive, the oxidation growth rate will be different than for bare copper environmentally aged for a similar duration of time. Therefore, water contact angles for each environmental test group were measured using special test specimens that mimicked the exposure of the copper bonding surface to similar amounts of oxygen and moisture as the interfacial fracture test specimens. These specimens used the same geometry as the interfacial fracture test specimens, but the underfill adhesive was cured separately in an individual mold. After curing the adhesive, the underfill was placed on top of the copper substrate and held in place by c-clamps. Similar to the interfacial fracture test specimens, a water-proof sealant was applied around the perimeter of the test specimen to eliminate

wicking of moisture at the interface and force 1D diffusion through the top surface of the underfill. After environmental preconditioning, the water-proof perimeter, c-clamps, and underfill were removed from the test specimen for contact angle measurement of the copper surface.

Experimentally measured water contact angle results were as follows: 76° for 85°C thermal aging, 76° for 85°C/50%RH moisture preconditioning, 77° for 85°C/65%RH moisture preconditioning, and 77° for 85°C/85%RH moisture preconditioning. All test groups were preconditioning for the same duration of 168 hours, which was the same criteria used in the evaluation of the effect of moisture on interfacial adhesion. Based on these results, it is evident that all levels of environmental preconditioning did not significantly alter the water contact angle and associated hydrophobicity of the interface. As a result, similar interfacial wetting characteristics of moisture at the interface will occur for all preconditioning environments.

Although the contact angle did not significantly change, there did appear to be a slight increase in the water contact angle with moisture preconditioning. Previous studies have shown both an increase [28,61] and decrease [7,25] in the water contact angle of copper with oxidation. The oxidation–reduction chemistry occurring at the interface relative to environmental preconditioning is complex, and the differences in trends could be attributed to the degree of oxidation altering the surface chemistry [7], change in surface roughness of the substrate from oxidation growth [25], and contamination of the surface by hydrocarbons from the environment [33]. In addition, Yi et al. [61] has provided data correlating the oxide layer thickness on copper leadframes to water contact angles. These data shows a slow, gradual increase in oxide thickness from water contact angles ranging from 72°–78°, but depicts a sharp increase in oxide layer thickness for contact angles exceeding 80°. Based on results for the water contact angle on copper in this study, all measurements yielded average contact angles less than 78° with vary little variation with each other. This indicates a similar level of interfacial hydrophobicity and oxide layer thickness for all environmentally preconditioned test groups. Both Mino et al. [35] and Chong et al. [8] have shown that the development of the copper oxide layer thickness is significantly slower and minimal for temperatures below 100°C and 120°C. Since the test specimens in this study had a temperature component of only 85°C, it is anticipated that the oxide layer thickness that developed on test specimens would have a minimal effect on toughness results. This is also supported by X-ray Photoelectron Spectroscopy (XPS) results. XPS showed the presence of cupric oxide not only in the 85°C/50%RH, 85°C/65%RH, and 85°C/85%RH test groups, but also in the 85°C thermal aging test group. As a result, identical oxide chemical formations existed at the interface for all environmentally preconditioned test groups. In addition, similar atomic percentages of cupric oxide were obtained when comparing thermal aging at 85°C to the moisture preconditioning environments of 85°C/50%RH, 85°C/65%RH, and 85°C/85%RH, indicating that the moisture component had a minimal contribution to oxidation growth rates on the copper compared to the available oxygen in the air common to all environmental preconditioned environments. Consequently, a similar level of oxidation thickness existed on all environmentally preconditioned test specimens, which supports the results from the water contact angle measurements.

Since oxides were removed from the copper surface before adhesive bonding and the flux present in the no-flow underfill would have removed any oxides that developed during adhesive curing, it is possible that the oxidation growth from environmental preconditioning would have an effect on the interfacial fracture toughness results. This oxide growth could displace the underfill from the copper substrate after bonding to contribute to the observed loss in adhesion after moisture preconditioning shown in Figure 17.15. Since both

water contact angle measurements and XPS results demonstrate a similar oxidation thickness existed on all environmentally preconditioned test specimens, the 85°C thermal aging results can be compared to the control test results to ascertain the effect of oxidation growth on the loss in adhesion without the contribution from moisture. As shown in Figure 17.15, thermal aging at 85°C produced little to no effect on interfacial fracture toughness results, thus oxidation growth displacing the underfill after adhesive bonding had an insignificant effect on the adhesion loss compared to the effect of moisture from moisture preconditioning.

17.4.4. Interfacial Fracture Toughness Recovery from Moisture Uptake

The underfill/copper interface was found to be very sensitive to moisture, with large decreases in interfacial fracture toughness occurring for moisture preconditioning environments of 85°C/50%RH, 85°C/65%RH, and 85°C/85%RH (Figure 17.15). To further investigate the reversible and irreversible nature of moisture on the interfacial adhesion of the underfill/copper interface, additional test specimens were moisture preconditioned for each condition for 168 hours followed by baking at 95°C until fully dry. A fully dried state was established when there was no measurable change in the weight of a specimen for a period of 24 hours. Upon reaching a dry state, specimens were fracture tested to ascertain the interfacial fracture toughness. The entire range of mode mixity for all interfacial test specimens fell between $-37.43°$ to $-37.48°$. The substrate height was used to define the characteristic length for all reported toughness values when evaluating the mode mixity. Since the variation in mode mixity was negligible, the effect of this variation influencing interfacial fracture toughness results between different test groups is insignificant. Consequently, toughness recovery results for different moisture preconditioned test groups can be compared to one another to ascertain the effect of increasing moisture content on toughness values. Figure 17.21 provides a graphical depiction of the effect of environmental preconditioning and recovery of the underfill/copper interfacial fracture toughness.

As shown in Figure 17.21, most of the loss in interfacial fracture toughness from moisture was not recovered upon fully drying. Since the small change in the underfill elastic modulus from moisture was recoverable upon fully drying, the permanent reduction in the toughness of the underfill/copper interface is attributed to the direct presence of moisture at the interface debonding the underfill adhesive to the copper substrate. Similar in form to the recoverability of the elastic modulus given by Equation (17.9), the recoverability for the interfacial fracture toughness will be defined as follows:

$$\textit{Recoverability}\ (\%) = \frac{G_{c,recovery} - G_{c,sat}}{G_{c,dry} - G_{c,sat}} \cdot 100, \tag{17.19}$$

where $G_{c,recovery}$ is value of the interfacial fracture toughness upon fully drying from the moisture saturated state, $G_{c,sat}$ is the saturated value of the interfacial fracture toughness after moisture absorption, and $G_{c,dry}$ is the unaged, control value of the interfacial fracture toughness. Equation (17.19) only applies when the mode mixity of the interfacial fracture toughness before and after moisture preconditioning remains relatively unchanged, otherwise changes in the toughness due to a contribution from a change in the mode mixity will introduce error in the recoverability results. The recoverability of the underfill/copper interfacial fracture toughness is given in Table 17.5.

As shown by Table 17.5, the irreversible damage on interfacial fracture toughness from exposure to moisture was substantial for the underfill/copper interface. Very little

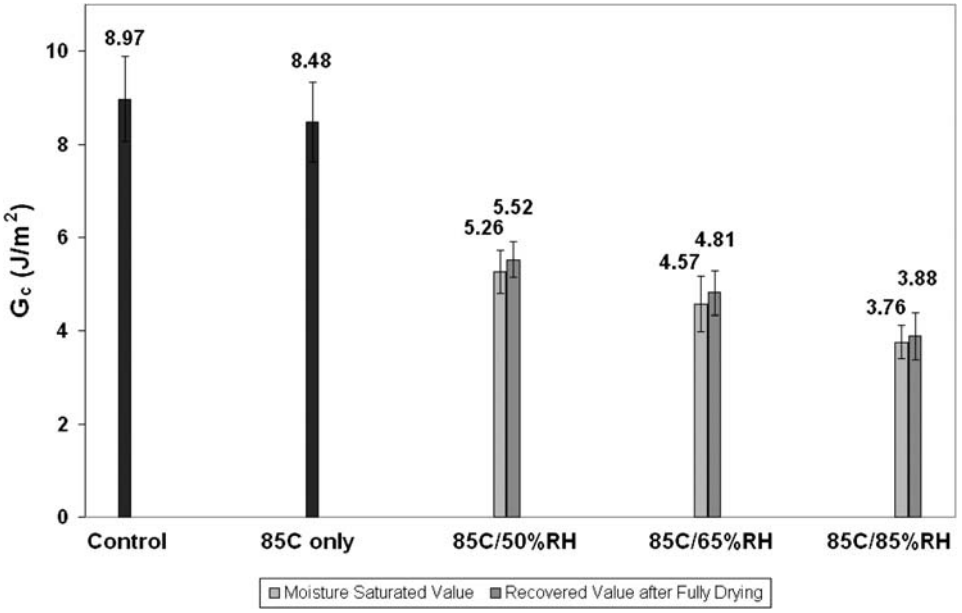

FIGURE 17.21. Recovery of the underfill/copper interfacial fracture toughness on removal of moisture.

TABLE 17.5.
Recoverability of the underfill/copper interfacial fracture toughness from moisture uptake after subsequent drying.

T (°C)	RH (%)	C_{sat} (wt%)	$G_{c,sat}$ (J/m^2)	$G_{c,recovery}$ (J/m^2)	*Recoverability* (%)
Control	—	0.00	8.97 ± 0.91	—	—
85	50	0.65	5.26 ± 0.47	5.52 ± 0.38	7.0
85	65	0.77	4.57 ± 0.58	4.81 ± 0.47	5.5
85	85	1.02	3.76 ± 0.36	3.88 ± 0.50	2.3

of the underfill/copper interfacial fracture toughness was recoverable after fully drying, with recoverability values for all moisture preconditioning environments less than 7%. It is also evident that a relatively small amount of moisture reaching the interface causes the structural integrity of the adhesive bond to be noticeably, permanently compromised.

17.4.5. Interfacial Fracture Toughness Moisture Degradation Model

Having implemented an extensive experimental program to ascertain the role of moisture in adhesion degradation and the physical mechanisms responsible for the change in interfacial adhesion, the focus now shifts to developing a model depicting the intrinsic loss in interfacial fracture toughness as a function of the critical parameters relevant to moisture. At the root of this model is characterizing the dominant mechanism for adhesion between the adhesive and substrate. There are four primary mechanisms for adhesion which have been proposed. They include mechanical interlocking, diffusion theory, electronic theory, and adsorption theory [30]. For the underfill/copper interface, the contributions of interfacial diffusion and electrostatic forces between the adhesive and substrate causing

adhesion is far lower than the effects of mechanical interlocking and adsorption. Since the copper substrates in this study were polished to a mirror finish, the effects from mechanical interlocking of the adhesive into irregularities present on the substrate surface will be small compared to the effects from intermolecular secondary forces (i.e., Van der Waals) between the atoms and molecules in the surfaces of the adhesive and substrate. Consequently, adsorption theory will dominate the adhesive bonding at the underfill/copper interface of our test specimens.

Provided adsorption theory governs adhesion and only secondary forces are acting across an interface, the stability of an adhesive/substrate interface in the presence of moisture can be ascertained from thermodynamic arguments. The thermodynamic work of adhesion, W_A, in an inert medium is given by [30]:

$$W_A = \gamma_a + \gamma_s - \gamma_{as}, \tag{17.20}$$

where γ_a is the surface free energy of the adhesive, γ_s is the surface free energy of the substrate, and γ_{as} is the interfacial free energy. In the presence of a liquid, the thermodynamic work of adhesion, W_{Al}, is given by:

$$W_{Al} = \gamma_{al} + \gamma_{sl} - \gamma_{as}, \tag{17.21}$$

where γ_{al} and γ_{sl} are the interfacial free energies between the adhesive/liquid and substrate/liquid interfaces, respectively. Typically the thermodynamic work of adhesion of an adhesive/substrate interface in an inert medium, W_A, is positive, which indicates the amount of energy required to separate a unit area of the interface. However, the thermodynamic work of adhesion in the presence of a liquid, W_{Al}, can be negative, which indicates the interface is unstable and will separate when it comes in contact with the liquid. Thus, the calculation of W_A and W_{Al} can indicate the environmental stability of the adhesive/substrate interface. Kinloch [30] has shown that W_A and W_{Al} may be calculated from the following expressions:

$$W_A = 2\sqrt{\gamma_a^D \gamma_s^D} + 2\sqrt{\gamma_a^P \gamma_s^P}, \tag{17.22}$$

$$W_{Al} = 2(\gamma_{lv} - \sqrt{\gamma_a^D \gamma_{lv}^D} - \sqrt{\gamma_a^P \gamma_{lv}^P} - \sqrt{\gamma_s^D \gamma_{lv}^D} - \sqrt{\gamma_s^P \gamma_{lv}^P} + \sqrt{\gamma_a^D \gamma_s^D} + \sqrt{\gamma_a^P \gamma_s^P}), \tag{17.23}$$

where γ^D is the dispersion component of surface free energy, γ^P is the polar component of surface free energy, and γ_{lv} is the surface free energy of the liquid. Table 17.6 gives the polar and dispersion surface free energies of epoxy, copper, and water.

TABLE 17.6.
Polar and dispersion surface free energies of epoxy, copper, and water [30].

Substance	γ (mJ/m^2)	γ^D (mJ/m^2)	γ^P (mJ/m^2)
Epoxy	46.2	41.2	5.0
Copper	1360	60	1300
Water	72.2	22.0	50.2

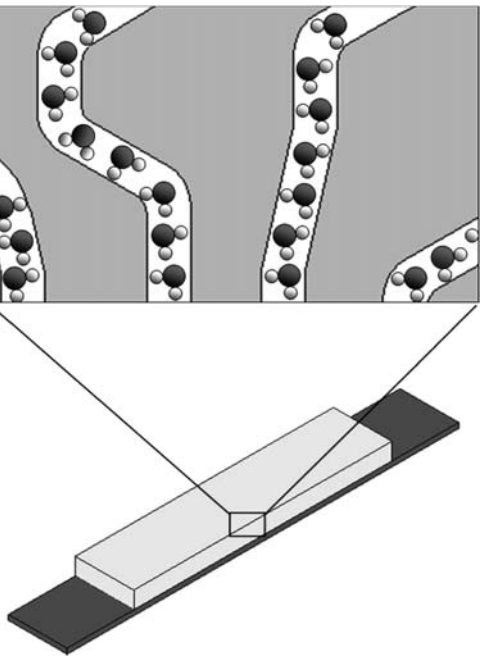

FIGURE 17.22. Moisture transport through the bulk epoxy of an interfacial fracture test specimen.

Using the values given in Table 17.6 and substituting into Equation (17.22), the thermodynamic work of adhesion of the epoxy/copper interface is 260.7 mJ/m^2. If water is present at the epoxy/copper interface, the thermodynamic work of adhesion given by Equation (17.23) is -270.4 mJ/m^2. Therefore, since the work of adhesion is positive before exposure to moisture and negative after exposure, all adhesion of the epoxy/copper interface is lost if water comes in contact with the interface. This is supported by the recovery interfacial fracture toughness results presented in Section 17.4.4, where virtually none of the observed loss in adhesion from moisture exposure was recovered upon fully drying.

Using adsorption theory as the physical basis for the loss in adhesion from moisture, expressions are now developed depicting the amount of moisture delivered to the underfill/copper interface. Since the interfacial fracture test specimens were designed to prevent wicking of moisture at the interface and the copper substrate provides a barrier for moisture transport, the moisture transport to the interface is governed by the epoxy network of the underfill. Soles and Yee [48] have shown that water traverses within the epoxy through the network of nanopores inherent in the epoxy structure. A typical nanopore ranges from 5.0 to 6.1 Å in diameter. Figure 17.22 illustrates the transport of moisture through the bulk epoxy of an interfacial fracture test specimen.

Assuming that the nanopore channels are the only mechanism by which moisture can be delivered to the interface, the saturation concentration in the epoxy expressed in mg H_2O/mm^3 is given by:

$$C_{sat} = \frac{\rho(NV)}{V_{tot}}, \tag{17.24}$$

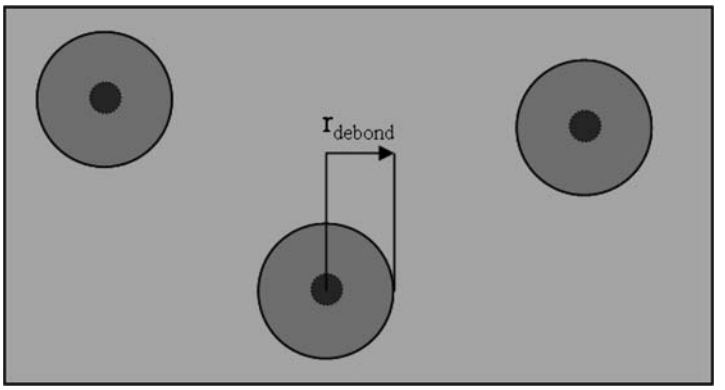

FIGURE 17.23. Graphical illustration of the parameter, r_{debond}, at the interface.

where ρ is the density of water measured in milligram per cubic millimeter (mg/mm^3), N is the number of nanopores actively participating within the epoxy network, V is the volume occupied by a single nanopore in the epoxy network, and V_{tot} is the total volume of the epoxy. After rearrangement of Equation (17.24), the number of nanopores actively participating within an epoxy system for a given saturation concentration is as follows:

$$N = \frac{4AC_{sat}}{\pi \rho D^2}, \tag{17.25}$$

where A is the total area of the interface and D is the nanopore diameter. Assuming adsorption theory holds, the adhesive bond area, A_{bond}, that remains intact after exposure to moisture will depend on the area occupied by the moisture at the interface, A_{H_2O}:

$$A_{bond} = A - A_{H_2O}. \tag{17.26}$$

Relating this adhesive bond area to the number of nanopores actively participating in transport yields:

$$A_{bond} = A - \pi N r_{debond}^2, \tag{17.27}$$

where r_{debond} represents the debond radius of moisture at the interface that occurs at each nanopore. The debond radius must be greater or equal to the nanopore radius and is governed by the interfacial hydrophobicity of the adhesive/substrate interface. Figure 17.23 provides a graphical depiction of the parameter, r_{debond}, at the interface.

Substituting Equation (17.25) into (17.27) provides an expression for the adhesive bond area that remains intact after exposure to a particular moisture saturation concentration:

$$A_{bond} = A - \frac{4AC_{sat} r_{debond}^2}{\rho D^2}. \tag{17.28}$$

We now want to employ a fracture mechanics development to relate the change in bond area due to the presence of moisture at the interface. Recall from fracture mechanics the general form of the stress intensity factor:

$$K = S\sigma\sqrt{\pi a}, \tag{17.29}$$

where S is a dimensionless constant that depends on the geometry and mode of loading, σ is the remotely applied stress, an a is the crack length. The stress intensity factor is related to the fracture toughness, G_c, by the following expression:

$$G_c = Z\sigma^2, \tag{17.30}$$

where

$$Z = \frac{\pi a S^2(1-\upsilon^2)}{E}.$$

Based on the thermodynamic work of adhesion for the epoxy/copper interface, the interface will become unstable and debond in the presence of moisture; however, since interfacial fracture toughness is a material property that characterizes the adhesion of the interface, the toughness must be the same in all areas that remain bonded after exposure to moisture. Using mode I loading and making the following three assumptions: (1) Adsorption theory dominates the interfacial bonding; (2) The change in the mechanical properties of both the adhesive and substrate from moisture is small relative to the change in bond area from moisture, and (3) The relative change in fracture toughness from moisture remains constant irrespective to the means of measuring the toughness for a given moisture saturation concentration, an expression is obtained relating the change in bond area due to the presence of moisture to the change in the critical load of fracture:

$$\frac{P_{wet}}{A - \pi N r_{debond}^2} = \frac{P_{dry}}{A}. \tag{17.31}$$

Rearranging Equation (17.31) to obtain an expression for P_{wet} and substituting that value into Equation (17.30) for the wet, saturated case yields the following expression:

$$G_{c,wet} = \left(1 - \frac{\pi N r_{debond}^2}{A}\right)^2 G_{c,dry}. \tag{17.32}$$

As the saturation moisture concentration increases, so will the number of active nanopores participating. The incremental change in fracture toughness due to the participation of a single additional nanopore, $N+1$, is given by:

$$G_{c,wet} = \left(1 - \frac{\pi (N+1) r_{debond}^2}{A}\right)^2 G_{c,dry}. \tag{17.33}$$

For convenience, define f such that for N nanopores participating:

$$f_N = \frac{\pi N r_{debond}^2}{A}. \tag{17.34}$$

For $N+1$ nanopores participating:

$$f_{N+1} = \frac{\pi r_{debond}^2}{A}(N+1). \tag{17.35}$$

Restating Equations (17.32) and (17.33) in terms of f:

$$G_{c,wet}(f_N) = \left(1 - \frac{\pi N r_{debond}^2}{A}\right)^2 G_{c,dry}, \tag{17.36}$$

$$G_{c,wet}(f_{N+1}) = \left(1 - \frac{\pi r_{debond}^2}{A}\right)^2 G_{c,wet}(f_{N_N}). \tag{17.37}$$

Subtracting (17.36) from (17.37) and dividing by $f_{N+1} - f_N$ gives:

$$\frac{G_{c,wet}(f_{N+1}) - G_{c,wet}(f_N)}{f_{N+1} - f_N} = \frac{\left[1 - \left(\pi r_{debond}^2/A\right)\right]^2 G_{c,wet}(f_N) - G_{c,wet}(f_N)}{f_{N+1} - f_N}. \tag{17.38}$$

Utilizing a Taylor series expansion of f_N with first order accuracy and substituting Equations (17.34) and (17.35) into (17.38) yields:

$$\frac{dG_{c,wet}(f_N)}{df_N} = \frac{\left[1 - \left(\pi r_{debond}^2/A\right)\right]^2 G_{c,wet}(f_N) - G_{c,wet}(f_N)}{\left(\pi r_{debond}^2/A\right)}. \tag{17.39}$$

Simplification and elimination of higher order terms gives the following differential equation characterizing the loss in interfacial fracture toughness due to moisture:

$$\frac{dG_{c,wet}(f_N)}{df_N} = -2G_{c,wet}(f_N), \tag{17.40}$$

subject to the boundary condition:

$$G_{c,wet}(f_N = 0) = G_{c,dry}. \tag{17.41}$$

Solution of Equation (17.40) gives:

$$G_{c,wet} = G_{c,dry} \exp\left[\frac{-8C_{sat} r_{debond}^2}{\rho D^2}\right]. \tag{17.42}$$

Equation (17.42) characterizes the loss in interfacial fracture toughness from moisture in terms of key parameters relevant to moisture. Using the value for the density of water at room temperature (0.998 mg/mm^3), an average nanopore diameter of 5.5 Å, and the saturation concentration determined from the experimental portion of this study in conjunction with Equations (17.25) and (17.42), the number of active nanopores participating, N, and value of r_{debond} can be determined by the intrinsic response of the material system to each level of moisture preconditioning. The results are shown in Table 17.7.

TABLE 17.7.
Key parameters relevant to moisture for the underfill/copper interface.

Environment	Substrate	Adhesive	C_{sat} (mg H_2O/mm^3)	N	r_{debond} (mm)
85°C/50%RH	Copper	Underfill	0.0075	1.006×10^{13}	1.640×10^{-6}
85°C/65%RH	Copper	Underfill	0.0089	1.194×10^{13}	1.692×10^{-6}
85°C/85%RH	Copper	Underfill	0.0118	1.583×10^{13}	1.669×10^{-6}

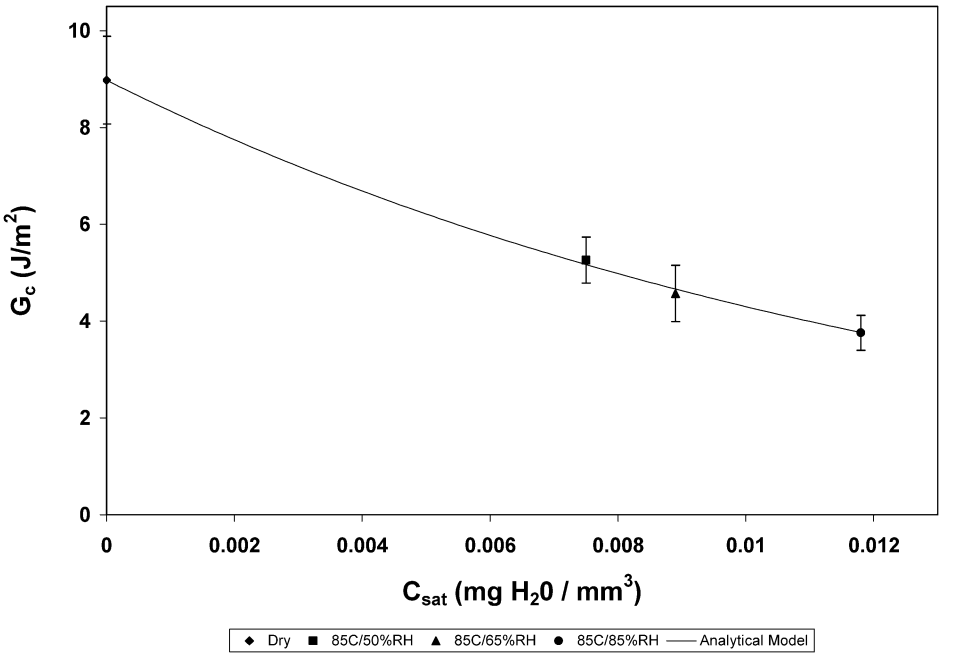

FIGURE 17.24. Analytical prediction of the loss in interfacial fracture toughness from moisture for the underfill/copper interface.

As shown in Table 17.7, the number of nanopores participating increases with saturation concentration. This is expected since an increase in saturation concentration would increase the available moisture for transport through the nanopores. In addition, the values for r_{debond} were similar for each moisture preconditioning environment for both respective interfaces, which is also expected since X-ray Photoelectron Spectroscopy and water contact angle results did not indicate a change in the interfacial hydrophobicity of the copper surface from moisture preconditioning. The slight variation in the values for r_{debond} could in part be attributed to experimental scatter. Since the results were similar, they were averaged to obtain a representative value for r_{debond} in the presence of moisture for each interface.

Using the moisture parameters identified for each interfacial material system, Equation (17.42) was used to predict the interfacial fracture toughness for the underfill/copper interface as a function of increasing saturation concentration.

As shown in Figure 17.24, Equation (17.42) accurately predicted the loss in interfacial fracture toughness as a function of increasing moisture concentration. Since Equa-

tion (17.42) was based on the physics of adsorption theory, it will yield a loss in interfacial fracture toughness provided there is moisture at the interface, no matter how small the concentration. This contradicts the results of previous studies, who have reported a critical concentration of water may exist below which there is no measurable loss in adhesion [10,23,31]. Based on the results of adsorption theory, it does not appear possible that a critical concentration of water could exist in theory. It is possible in those studies that other mechanisms for adhesion in addition to adsorption theory governed the adhesion at the interface, which could explain why a critical concentration of water was observed. An additional consideration is the method of testing used to obtain adhesion results. The aforementioned studies used lap shear test specimens to determine the interfacial strength after moisture preconditioning. Due to lacking a precrack at the interface and the applied load being distributed over the entire bonding area, these test specimens are not as sensitive to interfacial failure; consequently, possibly also explaining why in part a critical concentration of water appeared to exist for low concentrations of moisture. Conversely, interfacial fracture toughness test specimens are designed for interfacial failure through the use of a precrack at the interface, making them more sensitive to subtle changes in adhesion at the interface. The work of Wylde and Spelt [58] supports this observation. Using interfacial fracture toughness test specimens with a similar material system previously reported to exhibit a critical concentration of water from lap shear results, they found a decrease in the interfacial toughness from moisture for all concentrations of moisture, including those lower than the previously reported critical concentration of water. Consequently, provided adsorption theory dominates the adhesive bonding at the adhesive/substrate interface and the assumptions in the development of the model are satisfied, Equation (17.42) should accurately predict the loss in interfacial fracture toughness for a given moisture concentration.

REFERENCES

1. H. Ardebili, E.H. Wong, and M. Pecht, Hydroscopic swelling and sorption characteristics of epoxy molding compounds used in electronic packaging, IEEE Transactions on Components and Packaging Technologies, 26(1), pp. 206–214 (2003).
2. ASTM D790, Standard Test Methods for Flexural Properties of Unreinforced and Reinforced Plastics and Electrical Insulating Materials, Annual Book of ASTM Standards, Vol. 08.01, 1999.
3. D. Brewis, J. Comyn, A. Raval, and A. Kinloch, The effect of humidity on the durability of aluminum-epoxide joints, International Journal of Adhesion and Adhesives, 10, pp. 247–253 (1990).
4. F. Buehler and J. Seferis, Effect of reinforcement and solvent content on moisture absorption in epoxy composite materials, Composites: Part A: Applied Science and Manufacturing, 31, pp. 741–748 (2000).
5. L. Butkus, Environmental durability of adhesively bonded joints, Doctoral Thesis, Georgia Institute of Technology, Woodruff School of Mechanical Engineering, Atlanta, GA, 1997.
6. Y. Cengel and M. Boles, Thermodynamics: An Engineering Approach, McGraw-Hill, Inc., New York, 1994.
7. K. Cho and E. Cho, Effect of the microstructure of copper oxide on the adhesion behavior or epoxy/copper leadframe joints, Journal of Adhesion Science and Technology, 14(11), pp. 1333–1353 (2000).
8. C. Chong, A. Leslie, L. Beng, and C. Lee, Investigation on the effect of copper leadframe oxidation on package delamination, Proceedings of the 45th Electronic Components and Technology Conference, 1995, pp. 463–469.
9. P. Chung, M. Yuen, P. Chan, N. Ho, and D. Lam, Effect of copper oxide on the adhesion behavior of epoxy molding compound-copper interface, Proceedings of the 52nd Electronic Components and Technology Conference, 2002, pp. 1665–1670.
10. J. Comyn, C. Groves, and R. Saville, Durability in high humidity of glass-to-lead alloy joints bonded with and epoxide adhesive, International Journal of Adhesion and Adhesives, 14, pp. 15–20 (1994).
11. J. Crank, The Mathematics of Diffusion, Clarendon Press, Oxford, 1956.

12. A. Crocombe, Durability modeling concepts and tools for the cohesive environmental degradation of bonded structures, International Journal of Adhesion and Adhesives, 17, pp. 229–238 (1997).
13. X. Dai, M. Brillhart, and P. Ho, Adhesion measurement for electronic packaging applications using double cantilever beam method, IEEE Transactions on Components and Packaging Technology, 23, pp. 101–116 (2000).
14. X. Dai, M. Brillhart, M. Roesch, and P. Ho, Adhesion and toughening mechanisms at underfill interfaces for flip-chip-on-organic-substrate packaging, IEEE Transactions on Components and Packaging Technology, 23(1), pp. 117–127 (2000).
15. B. DeNeve and M. Shanahan, Effects of humidity on an epoxy adhesive, International Journal of Adhesion and Adhesives, 12, pp. 191–196 (1992).
16. H. Dodiuk, L. Drori, and J. Miller, The effect of moisture in epoxy film adhesives on their performance: I. Lap shear strength, Journal of Adhesion, 17, pp. 33–44 (1984).
17. L. Fan, C. Tison, and C. Wong, Study on underfill/solder adhesion in flip-chip encapsulation, IEEE Trans. on Advanced Packaging, 25(4), pp. 473–480 (2002).
18. T. Ferguson and J. Qu, Elastic modulus variation due to moisture absorption and permanent changes upon redrying in an epoxy based underfill, IEEE Transactions on Components and Packaging Technologies, 29(1), pp. 105–111 (2006).
19. T. Ferguson and J. Qu, Moisture and temperature effects on the reliability of interfacial adhesion of a polymer/metal interface, Proceedings of the 54th Electronic Components and Technology Conference, 2004.
20. T. Ferguson and J. Qu, Moisture absorption analysis of interfacial fracture test specimens composed of no-flow underfill materials, ASME Journal of Electronic Packaging, 125, pp. 24–30 (2003).
21. T. Ferguson and J. Qu, Effect of moisture on the interfacial adhesion of the underfill/soldermask interface, ASME Journal of Electronic Packaging, 124, pp. 106–110 (2002).
22. T. Ferguson and J. Qu, Moisture absorption in no-flow underfills and its effect on interfacial adhesion to solder mask coated FR-4 printed wiring board, International Symposium and Exhibition on Advanced Packaging Materials, Processes, Properties, and Interfaces, 2001, pp. 327–332.
23. R. Gledhill, A. Kinloch, and J. Shaw, A model for predicting joint durability, Journal of Ahdesion, 11, pp. 3–15 (1980).
24. B. Harper and V. Kenner, Effects of temperature and moisture upon the mechanical behavior of an epoxy molding compound, ASME Advances in Electronic Packaging, 1, pp. 1207–1212 (1997).
25. K. Hong, H. Imadojemu, and R. Webb, Effects of oxidation and surface roughness on contact angle, Experimental Thermal and Fluid Science, 8, pp. 279–285 (1994).
26. J. Hutchinson and Z. Suo, Mixed mode cracking in layered materials, Advances in Applied Mechanics, Vol. 29, Academic Press, New York, 1992.
27. R. Jurf and J. Vinson, Effect of moisture on the static and viscoelastic shear properties of epoxy adhesives, Journal of Materials Science, 20, pp. 2979–2989 (1985).
28. S. Kim, The role of plastic package adhesion in IC performance, Proceedings of the 41st Electronic Components and Technology Conference, 1991, pp. 750–758.
29. J.K. Kim, M. Lebbai, J. Liu, J.H. Kim, and M. Yuen, Interface adhesion between copper lead frame and epoxy molding compound: effects of surface finish, oxidation, and dimples, Proceedings of the 50th Electronic Components and Technology Conference, 2000, pp. 601–608.
30. A.J. Kinloch, Adhesion and Adhesives Science and Technology, Chapman and Hall, London, 1987.
31. A. Kinloch, Interfacial fracture mechanical aspects of adhesive bonded joints—a review, Journal of Adhesion, 10, pp. 193–219 (1979).
32. H. Lee and J. Qu, Microstructure, adhesion strength and failure path at a polymer/roughened metal interface, Journal of Adhesion and Science Technology, 17(2), pp. 195–215 (2003).
33. S. Luo, Study on adhesion of underfill materials for flip chip packaging, Doctoral Thesis, Georgia Institute of Technology, School of Textile and Fibers Engineering, Atlanta, GA, 2003.
34. S. Luo and C.P. Wong, Influence of temperature and humidity on adhesion of underfills for flip chip packaging, Proceedings of the 51st Electronic Components and Technology Conference, 2001, pp. 155–162.
35. T. Mino, K. Sawada, A. Kurosu, M. Otsuka, N. Kawamura, and H. Yoo, Development of moisture-proof thin and large QFP with copper lead frame, Proceedings of the 48th Electeonic Components and Technology Conference, 1998, pp. 1125–1131.
36. R. Morgan, J. O'Neal, and D. Fanter, The effect of moisture on the physical and mechanical integrity of epoxies, Journal of Materials Science, 15, pp. 751–764 (1980).
37. R. Morgan, J. O'Neal, and D. Miller, The structure, modes of deformation and failure, and mechanical properties of diaminodiphenyl sulphone-cured tetragylcidyl 4,4′ diaminodiphenyl methane epoxy, Journal of Materials Science, 14, pp. 109–124 (1979).

38. A. Netravali, R. Fornes, R. Gilbert, and J. Memory, Effects of water sorption at different temperatures on permanent changes in an epoxy, Journal of Applied Polymer Science, 30, pp. 1573–1578 (1985).
39. S. Orman and C. Kerr, in D.J. Alner, Ed., Aspects of Adhesion, University of London Press, London, 1971.
40. A. Pasztor, in F. Settle, Ed., Handbook of Instrumental Techniques for Analytical Chemistry, Chapter 50, Prentice Hall, New Jersey, 1997.
41. B. Prime, in E. Turi, Ed., Thermal Characterization of Polymeric Materials, Vol. 2, Chapter 10, San Diego, Academic Press, San Diego, 1997.
42. S. Rosen, Fundamental Principles of Polymeric Materials, John Wiley and Sons, New York, 1993.
43. G. Shaw, C. Rogers, and J. Payer, The effect of immersion on the breaking force and failure locus in an epoxy/mild steel system, Journal of Adhesion, 38, pp. 255–268 (1992).
44. C.H. Shen and G.S. Springer, Moisture absorption and desorption of composite materials, Journal of Composite Materials, 10, pp. 2–20 (1976).
45. S. Shi and C.P. Wong, Study of the fluxing agent effects on the properties of no-flow underfill materials for flip-chip applications, Proceedings of the 48th Electronic Components and Technology Conference, 1998, pp. 117–124.
46. R. Shook and J. Goodelle, Handling of highly-moisture sensitive components—an analysis of low-humidity containment and baking schedules, Proceedings of the 49th Electronic Components and Technology Conference, 1999, pp. 809–815.
47. C. Soles, F. Chang, D. Gidley, and A. Yee, Contributions of the nanovoid structure to the kinetics of moisture transport in epoxy resins, Journal of Polymer Science: Part B: Polymer Physics, 38, pp. 776–791 (2000).
48. C. Soles and A. Yee, A discussion of the molecular mechanisms of moisture transport in epoxy resins, Journal of Polymer Science: Part B: Polymer Physics, 38, pp. 792–802 (2000).
49. N. Su, R. Mackie, and W. Harvey, The effects of aging and environment on the fatigue life of adhesive joints, International Journal of Adhesion and Adhesives, 9, pp. 85–91 (1992).
50. E. Suhir, Failure criterion for moisture-sensitive plastic packages of integrated circuit (IC) devices: application of von-Karman's equations with consideration of thermoelastic strains, International Journal of Solids and Structures, 34(23), pp. 2991–3019 (1997).
51. D. Suryanarayana, R. Hsiao, T. Gall, and J. McCreary, Enhancement of flip-chip fatigue life by encapsulation, IEEE Transactions on Components, Hybrids, and Manufacturing Technology, 14(1), pp. 218–223 (1991).
52. M. Uschitsky and E. Suhir, Moisture diffusion in epoxy molding compounds filled with particles, Journal of Electronic Packaging, 123, pp. 47–51 (2001).
53. M. Uschitsky and E. Suhir, Moisture diffusion in epoxy molding compounds filled with silica particles, ASME Structural Analysis in Microelectronics and Fiber Optics, 21, pp. 141–170 (1997).
54. M. Vanlandingham, R. Eduljee, and J. Gillespie, Moisture diffusion in epoxy systems, Journal of Applied Polymer Science, 71, pp. 787–798 (1999).
55. M. Wahab, A. Crocombe, A. Beevers, and K. Ebtehaj, Coupled stress-diffusion analysis for durability study in adhesively bonded joints, International Journal of Adhesion and Adhesives, 22, pp. 61–73 (2002).
56. E. Wong, K. Chan, T. Lim, and T. Lam, Non-fickian moisture properties characterization and diffusion modeling for electronic packages, Proceedings of the 49th IEEE Electronic Components and Technology Conference, 1999, pp. 302–306.
57. W. Wright, The effect of diffusion of water into epoxy resins and their carbon-fibre reinforced composites, Journal of Composites, 12, pp. 201–205 (1981).
58. J. Wylde and J. Spelt, Measurement of adhesive joint fracture properties as a function of environmental degradation, International Journal of Adhesion and Adhesives, 18, pp. 237–246 (1998).
59. G.Z. Xiao and M. Shanahan, Water absorption and desorption in an epoxy resin with degradation, Journal of Polymer Science: Part B: Polymer Physics, 35, pp. 2659–2670 (1997).
60. D. Yeung, M. Yuen, D. Lam, and P. Chan, Measurement of interfacial fracture toughness for microelectronic packages, Journal of Electronics Manufacturing, 10, pp. 139–145 (2000).
61. S. Yi, C. Yue, J. Hsieh, L. Fong, and S. Lahiri, Effects of oxidation and plasma cleaning on the adhesion strength of molding compounds to copper leadframes, Journal of Adhesion Science and Technology, 13, pp. 789–804 (1999).
62. O. Yoshioka, N. Okabe, S. Nagayama, R. Yamagishi, and G. Murakami, Improvement of moisture resistance in plastic encapsulants MOS-IC by surface finishing copper leadframe, Proceedings of the 39th Electronic Components and Technology Conference, 1989, pp. 464–471.
63. M. Zanni-Deffarges and M. Shanahan, Diffusion of water into an epoxy adhesive: comparison between bulk behaviour and adhesive joints, International Journal of Adhesion and Adhesives, 15, pp. 137–142 (1995).
64. M. Zanni-Deffarges and M. Shanahan, Bulk and interphase effects in aged structural joints, Journal of Adhesion, 45, pp. 245–257 (1994).